Fluid Phase Equilibria 598 (2025) 114479

Contents lists available at ScienceDirect

Fluid Phase Equilibria

journal homepage: www.journals.elsevier.com/fluid-phase-equilibria

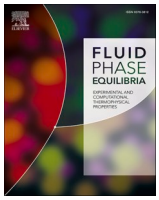

Modeling CO_2 solubility in deep eutectic solvents using the saft-vr mie and pc-saft equations of state

Cleiton S. Beraldo [a], Luis A. Follegatti-Romero [a,*], Georgios M. Kontogeorgis [b], Xiaodong Liang [b,*]

[a] Laboratory of Separation and Purification Engineering (LaSPE), Department of Chemical Engineering (PQI), Polytechnic School (EP), University of São Paulo (USP), São Paulo SP, Brazil

[b] Center for Energy Resources Engineering (CERE), Department of Chemical and Biochemical Engineering, Technical University of Denmark, DK–2800 Kgs. Lyngby, Denmark

ARTICLE INFO

Keywords:
Deep eutectic solvents
CO_2 solubility
SAFT-VR Mie
PC-SAFT
Combining rules

ABSTRACT

This study presents the first comparison of SAFT-VR Mie and PC-SAFT in modeling CO_2 solubility in Deep Eutectic Solvents (DESs). Experimental density data was used to adjust pure-component parameters (m, σ, and ε) for DESs in the SAFT models, whereas the unlike-segment interaction energy between CO_2 and the DES was either calculated with combining rules or optimized to reproduce experimental solubility data. A simplified Hudson-McCoubrey combining rule (ionization potentials assumed equal), applied for the first time to CO_2–DES systems, was compared with the conventional Lorentz-Berthelot rule. Four hydrophilic and six hydrophobic DESs were modeled as pseudo-pure components, either as non-associating or associating species, following 2B or 4C association schemes in both equations of state. It was found that the Lorentz-Berthelot rule is unsuitable for CO_2–DES phase equilibrium modeling, particularly for hydrophobic DESs, while the Hudson-McCoubrey rule provided excellent agreement with experimental data for both SAFT-VR Mie and PC-SAFT, performing comparably to models with unlike-segment interaction energy obtained empirically. The 2B and 4C association schemes produced accurate solubility predictions and demonstrated slightly superior performance compared to the inert approach, particularly in the case of hydrophobic DESs. Additionally, CO_2 was modeled as either a neutral component or with 2B cross-association with DES, showing no significant difference in results. Finally, Helmholtz energy contributions to the residual pressure of pure hydrophobic DESs were analyzed, revealing that while association effects were minor, they positively influenced CO_2 solubility predictions.

1. Introduction

Deep Eutectic Solvents (DESs) are mixtures composed of a hydrogen bond acceptor (HBA), often an ionic liquid such as choline chloride [1, 2], and a hydrogen bond donor (HBD), which can include compounds like urea [3], glycerol [4], or carboxylic acids [5]. The solvents have garnered significant attention in recent years due to their versatile applications in climate change mitigation [6] and various engineering fields [7–9]. Their unique physicochemical properties, such as low volatility, high thermal stability, and biodegradability, position them as promising candidates not only for carbon capture and sequestration but also for a wide range of industrial processes [10]. In engineering, DESs are increasingly being explored as green solvents that can replace conventional organic solvents in chemical synthesis [11], catalysis [12], and separation processes [13–15]. For instance, their tunable solvation capabilities have been examined to enhance reaction selectivity and efficiency in catalytic systems [16], while their high ionic conductivity [17] makes them attractive for use in energy storage devices such as batteries [18] and supercapacitors [19]. Furthermore, DESs have been shown to possess potential in the extraction and recovery of valuable metals [20], waste treatment [21], and as corrosion inhibitors in metal processing [22]. Despite these promising applications, a comprehensive understanding of the phase behavior of CO_2 in DES systems and the comparative performance of different modeling approaches remains limited, highlighting the need for systematic studies in this domain.

Several thermodynamic models, notably the SAFT-VR Mie (Statistical Associating Fluid Theory of Variable Range Mie potentials) [23–25] and PC-SAFT (Perturbed Chain SAFT) [26,27] equations of state (EoS),

* Corresponding authors.
E-mail addresses: follegatti@usp.br (L.A. Follegatti-Romero), xlia@kt.dtu.dk (X. Liang).

https://doi.org/10.1016/j.fluid.2025.114479
Received 2 April 2025; Received in revised form 23 May 2025; Accepted 23 May 2025
Available online 24 May 2025

have been developed to predict phase equilibria and thermodynamic properties in complex fluid mixtures. However, direct comparisons of these models for DESs remain limited, despite the variety of available theoretical frameworks. Such studies are considered essential for identifying the most consistent and predictive models, especially when different assumptions and computational strategies are employed.

A key factor within these models is the choice of combining rules – such as the Hudson-McCoubrey (HM) [28] and the Lorentz-Berthelot (LB) [29] rules – which significantly influence solubility prediction and other thermodynamic properties in CO_2–DES mixtures. These rules can lead to substantial differences in predictions, directly impacting process design and optimization.

An alternative approach involves using experimental solubility data to adjust the CO_2–DES unlike interaction energy parameter in the SAFT model. While this method can enhance model agreement with empirical observations, it reduces the overall predictivity of the models by introducing a system-specific parameter that may not be transferable across different conditions. This dependency on fitted parameters is considered another critical gap in the literature, where the balance between accuracy and generality remains a challenging issue [7].

Table 1 summarizes key theoretical research contributions on CO_2 solubility in DESs using EoS, with PC-SAFT identified as the most commonly employed model, followed by soft-SAFT and CPA (Cubic-Plus-Association) EoS. In studies treating DESs as pseudo-pure components, the common approach assumes solvents with two association sites: one for the proton donor (H) and one for the electron pair donor (e). A major challenge in these models is their dependance on interaction parameters that are fitted to experimental solubility data in order to achieve accurate predictions. Additionally, the Lorentz-Berthelot rule is the most frequently used combining rule for modeling the CO_2–DES unlike-segment interaction energy parameter. Notably, some SAFT-based studies mistakenly refer to the 'combining rule' as the 'mixing rule.'

As shown in Table 1, both the individual-component and pseudo-pure approaches appear to be equally prevalent in the literature. The individual-component approach offers higher modeling fidelity by preserving the molecular identity of each constituent; however, it typically requires a more extensive parameter set and a broader experimental dataset compared to the simplified pseudo-pure method. Before committing to a rigorous individual-component approach, several models and methods can be explored using a simpler pseudo-pure description. Given that thermodynamic modeling of DESs is still in its early stages, ongoing research is focused on identifying optimal methods. One outstanding issue is the need for a deeper understanding of how DES self-association influences thermodynamic properties and the number of association sites formed. For example, the COSMO-RS (Conductor-like Screening Model for Real Solvents) was applied by Ojeda et al. [41] to assign two association sites to DESs – composed of tetraalkylammonium bromide or chloride (HBAs) and levulinic acid (HBD) – based on the charge distribution of their hydrogen bonding regions (σ-profiles). The solubility of CO_2 and SO_2 in DESs was then modeled, treating them as pseudo-pure components within the soft-SAFT framework. Segment parameters were fitted to experimental pure liquid density data. However, accurate predictions required the introduction of a temperature-independent binary interaction parameter (BIP), which was fitted against experimental solubility data.

Another open question concerns the interaction of DESs with CO_2. The CPA EoS was employed by Haghbakhsh and Raeissi [34] to investigate five cross-association strategies for CO_2 – treating it as an inert compound, a solvation-induced associate, or as an associating compound under the 2B, 3B, or 4C association schemes [45]. Phase equilibria were examined for 15 DESs, modeled as pseudo-pure components under the 2B scheme, with segment parameters optimized to experimental pure liquid density data. The findings suggest that both inert and solvation association schemes can appropriately describe CO_2 behavior, provided that a temperature-dependent BIP is used for accurate predictions.

More recently, a pseudo-pure component approach with the PC-SAFT EoS under the 2B association scheme was applied by Parvaneh et al. [38] to investigate CO_2 solubility in DESs. Two cross-association strategies for CO_2 – non-associating (inert) and associating (2B) – were compared, with DES segment parameters determined from pure liquid density data and association parameters fixed based on established PC-SAFT trends. A study of 109 CO_2–DES systems revealed significant deviations when no fitted BIPs were applied. To address these discrepancies, a temperature-dependent BIP was introduced, highlighting the need for novel predictive strategies that reduce reliance on empirical parameter fitting.

In this work, we address key research gaps by conducting a comprehensive comparative study of CO_2–DES phase equilibria using the SAFT-VR Mie and PC-SAFT equations of state. Leveraging the open-source thermodynamic toolkit *Clapeyron.jl* [46], we evaluate 10 CO_2–DES phase equilibrium systems, treating DESs as pseudo-pure compounds. We systematically explore the impact of different combining rules and the trade-offs involved in obtaining interaction energies empirically from phase equilibria data. Furthermore, three

Table 1
Summary of CO_2–DES phase equilibria modeling in literature (Ref. [30–44]) using equations of state.

Year	Equation of State	Combining rule [a]	Model type [b]	Parameter estimation [c]	N_{sites} [d]	DES description	Ref.
2014	PR	–	Correlative	Phase equilibria	–	pseudo-pure	[33]
2016	PC-SAFT	LB	BIP	Pure liquid density (ρ_L)	1H + 1e	pseudo-pure and individual-component	[35]
2017	soft-SAFT	LB	BIP	ρ_L	1H + 1e	pseudo-pure and individual-component	[43]
2017	PC-SAFT; PR, SRK	LB	BIP	ρ_L	1H + 1e	pseudo-pure	[44]
2017	PC-SAFT	LB	Predictive	ρ_L	1H + 1e	pseudo-pure	[32]
2018	soft-SAFT	LB	BIP	ρ_L	1H + 1e	individual-component	[41]
2018	CPA	–	BIP	ρ_L	1H + 1e	pseudo-pure	[34]
2019	soft-SAFT	LB	BIP	ρ_L	3H + 2e	individual-component	[42]
2020	soft-SAFT	LB	BIP	ρ_L	3H + 2e	individual-component	[37]
2020	PC-SAFT	LB	BIP	ρ_L	1H + 1e	pseudo-pure and individual-component	[39]
2021	PC-SAFT	LB	BIP	ρ_L	1H + 1e	pseudo-pure	[40]
2022	CPA, PR	–	BIP	ρ_L	1H + 1e	pseudo-pure and individual-component	[30]
2022	PC-SAFT	LB	BIP	ρ_L	1H + 1e	pseudo-pure	[31]
2022	PC-SAFT	LB	BIP	ρ_L	1H + 1e	pseudo-pure	[38]
2024	PC-SAFT	LB	BIP	ρ_L	no association	pseudo-pure	[36]

[a] Combining rule used in SAFT models to calculate the model parameter expressing the CO_2–DES unlike-segment interaction energy (ε_{ij}). The Lorentz-Berthelot (LB) rule [29] has been applied in all mentioned studies.

[b] Correlative: Experimental and estimated properties are identical. BIP: A binary interaction parameter governing the energy between CO_2 and DES segments was fitted using experimental solubility data. Predictive: ε_{ij} is determined solely through combining rules.

[c] Properties used in parameter estimation are listed.

[d] Number of association sites (N_{sites}): The values for H and e represent the number of proton and electron pair donors, respectively.

approaches for representing DES association are compared: treating the compound as non-associating (NA strategy) or modeling it using the 2B or 4C association schemes, which capture specific hydrogen bonding interactions. The contribution of association to the residual pressure is also examined. Through this study, we aim to refine optimal modeling strategies for DES-based CO_2 capture systems and improve predictive capabilities of these thermodynamic models.

2. Theory

2.1. SAFT-VR mie and pc-saft

The reduced residual Helmholtz energy (a_{res}) in the SAFT-VR Mie [23–25] and PC-SAFT [26,27] equations of state is generalized as the sum of contributing forces, as expressed:

$$a_{res} = a_{HS} + a_{disp} + a_{chain} + a_{assoc} \tag{1}$$

where a_{HS} is the hard-sphere contribution (reference term), a_{disp} is the dispersion contribution, a_{chain} is the chain contribution, and a_{assoc} is the association contribution.

The dispersion contribution describes the attractive van der Waals interactions between particles (i.e., London dispersion forces). In both SAFT-VR Mie and PC-SAFT, the calculation is based on Barker-Henderson perturbation theory [47,48]. The general expression for the dispersion energy is as follows:

$$a_{disp} = \sum_{n=1}^{\infty} a_n \tag{2}$$

In practice, the dispersion is truncated at the second-order term for PC-SAFT and at the third-order term for SAFT-VR Mie. In PC-SAFT, the dispersion contribution to the Helmholtz energy assumes a Lennard-Jones perturbing potential [26], while in SAFT-VR Mie, it is derived from a generalized Lennard-Jones potential (Mie potential) [24,49]:

$$u(r) = \frac{\lambda_r}{\lambda_r - \lambda_a}\left(\frac{\lambda_r}{\lambda_a}\right)^{\frac{\lambda_a}{\lambda_r-\lambda_a}} \epsilon\left[\left(\frac{\sigma}{r}\right)^{\lambda_r} - \left(\frac{\sigma}{r}\right)^{\lambda_a}\right] \tag{3}$$

where r is the distance between two particles, ϵ is the depth of the potential well, σ is the distance at which the potential is zero, λ_r and λ_a are the repulsive and attractive exponents, respectively.

The association contribution describes the specific, directional interactions between associating sites (e.g., hydrogen bonding). The system is modeled using the Wertheim TPT1 approach [50,51] for S bonding site types and N_A sites of type A:

$$a_{assoc} = \sum_{A=1}^{S} N_A\left(\ln X_A - \frac{X_A}{2} + \frac{1}{2}\right) \tag{4}$$

where X_A is the fraction of molecules not bonded at site of type A. The fraction X_A is determined by solving the following association equilibrium expression (mass-action equation) [24]:

$$X_A + \rho X_A \sum_{B=1}^{S} N_B X_B \Delta_{AB} = 1 \tag{5}$$

where ρ is the number density. Δ_{AB} represents the association strength between sites A and B. While the specific form of this function may vary across different SAFT equations of state, it can generally be expressed as:

$$\Delta_{AB} = F_{AB} K_{AB} I_{AB} \tag{6}$$

where F_{AB} is the Mayer function for the bonding interaction [52], K_{AB} denotes the length scale of the interaction [53], and I_{AB} represents the probability that the sites are correctly oriented to allow for overlap [54]. The PC-SAFT model follows the CK-SAFT (Chen and Kreglewski SAFT) [45,55] approach for association bonds, which depends on the hard sphere radial distribution function g_{HS} [56] and a dimensionless association volume κ_{AB}, reduced by the segment size σ:

$$\Delta_{AB}^{PC-SAFT} = F_{AB}\sigma^3 \kappa_{AB} g_{HS} \tag{7}$$

The SAFT-VR Mie EoS used in this work employs the association strength formulation proposed by Dufal et al. (2015) [25], which is based on a bonding volume with units of volume (Lennard-Jones kernel):

$$\Delta_{AB}^{SAFT-VRMie} = F_{AB} K_{AB} I(\varepsilon, \sigma) \tag{8}$$

where $I(\varepsilon,\sigma)$ represents the dimensionless association kernel which is function of segment energy ε (usually expressed as ε/k_B, in Kelvin, k_B being the Boltzmann constant) and segment size σ.

2.2. Combining rules

In SAFT modeling, selecting an appropriate combining rule is essential for determining how intermolecular interaction parameters for unlike pairs (ij) are derived from pure-component parameters. Two commonly used rules are the classical Lorentz-Berthelot rule (LB) [29] and the Hudson-McCoubrey rule (HM) [28], which differ in complexity and their treatment of molecular structure. For calculating the unlike-size parameter (σ_{ij}) between CO_2 (species i) and DES (species j), the Lorentz combining rule [57] is employed in both PC-SAFT and SAFT-VR Mie models.

$$\sigma_{ij} = \frac{1}{2}(\sigma_i + \sigma_j) \tag{9}$$

To ensure a 'fair' comparison between PC-SAFT and SAFT-VR Mie, the unlike-segment energy (ε_{ij}) was calculated using both the widely adopted Berthelot combining rule [58] (Eq. (10)) – which, when used in conjunction with Eq. (9), is referred to as the Lorentz-Berthelot (LB) combining rule [29] – and a simplified version of the Hudson-McCoubrey (HM) combining rule (Eq. (11)) [59]. In the latter, the ionization potentials of species i and j are assumed to be equal, and thus excluded from the expression. This assumption limits the applicability of the rule to systems where the ionization potentials are considered similar, but makes it more practical for general use, especially in cases where ionization potentials – such as for deep eutectic solvents – are not readily available.

$$\varepsilon_{ij}^{LB} = \sqrt{\varepsilon_i \varepsilon_j} \tag{10}$$

$$\varepsilon_{ij}^{HM} = \frac{\sqrt{\sigma_i^3 \sigma_j^3}}{\sigma_{ij}^3}\sqrt{\varepsilon_i \varepsilon_j} \tag{11}$$

In Eq. (11), the cross-interaction energy is modulated not only by the geometric mean of the pure-component energies but also by a factor dependent on the relative volumes (via σ^3) of the interacting species, thereby accounting for the molecular size differences between CO_2 and DES.

Instead of being calculated with combining rules, experimental phase equilibrium data can be used to fit ε_{ij}. While this approach reduces the predictive capability of the model, it yields more accurate results and allows for the determination of an 'optimal' ε_{ij} for each system, denoted as ε_{ij}^{fit}.

A common metric used to compare the ε_{ij} obtained from combining rules (ε_{ij}^{CR}) with ε_{ij}^{fit} is k_{ij}, which is widely employed in PC-SAFT and other models that utilize Eq. (10). It is typically referred to as the binary interaction parameter (BIP). In contrast, SAFT-VR Mie conventionally relies on Eq. (11), where k_{ij} is not explicitly included in the formulation. Nonetheless, k_{ij} serves as a useful comparative indicator between the empirically obtained unlike-segment interaction energy and the one derived from pure-component data.

$$k_{ij} = 1 - \frac{\varepsilon_{ij}^{\text{fit}}}{\varepsilon_{ij}^{\text{CR}}} \tag{12}$$

The cross-association between CO_2 and DES has also been considered in recent studies [37,38,40,42,60–63]. In this work, the CR1 combining rules, as assigned by Kontogeorgis (2004) [64], are employed, with Eq. (13) being used for the association energy and Eq. (14) for the association volume [65].

$$\varepsilon_{A_iB_j} = \frac{1}{2}\left(\varepsilon_{A_iB_i} + \varepsilon_{A_jB_j}\right) \tag{13}$$

$$K_{A_iB_j} = \sqrt{K_{A_iB_i}K_{A_jB_j}} \tag{14}$$

where A_i and B_j are the association site A in species i and the association site B in species j, respectively.

3. Methodology

3.1. DESs investigated

The molar ratio of the HBA and HBD in DES is known to influence CO_2 solubility, as it affects the ability of the solvent to interact with and stabilize CO_2 molecules [2,66]. An optimal ratio is known to enhance the formation of hydrogen bonds, thereby increasing CO_2 solubility. Conversely, a skewed ratio is associated with a reduction in the efficiency of these interactions, potentially decreasing the capacity of the solvent to dissolve CO_2. Thus, the determination of the precise molar ratio is considered crucial for maximizing the performance of DESs for CO_2 absorption [42,60]. The abbreviation, name, compound identification, and molecular weight (M_w) of the HBA and HBD present in the DESs studied are presented in Table 2. The DES is denoted using the format $[HBA^+][HBA^-]$:HBD (n_{HBA}:n_{HBD}), where n_{HBA}:n_{HBD} specifies the molar ratio of HBA and HBD.

As outlined in the Introduction, the DES solvents selected for this study were chosen based on their ability to achieve sufficient CO_2 solubility, a key criterion for effective carbon capture. All the DESs investigated in this work, along with their experimental density ranges, are listed in Table 3, as reported in the literature. Moreover, Table 4 summarizes the experimental CO_2 solubility data for these DESs, also sourced from the literature. All properties are evaluated against literature data using the average absolute relative deviation (%AARD), defined as follows:

$$\%\text{AARD} = \frac{100}{N_{\text{dp}}}\sum_{i=1}^{N_{\text{dp}}}\left(\frac{\left|z_i^{\text{cal}} - z_i^{\text{exp}}\right|}{z_i^{\text{exp}}}\right) \tag{15}$$

Table 2
Basic information of the hydrogen bond acceptors and hydrogen bond donors used in this work.

Abbreviation	Name	PubChem CID [67]	M_w (g/mol)
Hydrogen bond acceptor cation (HBA^+)			
Ch	Choline	305	104.17
TBA	TetraButylAmmonium	16028	242.46
TBP	TetraButylPhosphonium	75312	259.43
TPPP	TriPhenyl(2-Propenyl) Phosphonium	197741	303.40
MTA	MethylTricaprylylAmmonium	21219	368.70
TOA	Tetra-n-OctylAmmonium	2734118	466.90
Hydrogen bond acceptor anion (HBA^-)			
Cl	Chloride ion	312	35.45
Br	Bromide ion	259	79.90
Hydrogen bond donor (HBD)			
EG	Ethylene Glycol	174	62.07
Ph	Phenol	996	94.11
CA	Capric Acid	2969	172.26

where N_{dp} denotes the number of datapoints for the property z_i, with cal and exp superscripts expressing the calculated and experimental values, respectively.

3.2. Parameter estimation

In this section, a parameter estimation procedure for the PC-SAFT and SAFT-VR Mie modeling of DESs is presented. The focus is on estimating three key parameters: the segment number (m), the segment diameter (σ), and the segment energy (ε). Owing to the inherent experimental challenges associated with these compounds – namely, their low vapor pressures – the present approach relies predominantly on pure specific density experimental data.

Density data, measured across a wide temperature range (Table 3), serve as the primary input for the estimation procedure. This methodology is well-supported in the literature for both ionic liquids [72–74] and DESs (Table 1), due to the inherent challenges associated with their extremely low vapor pressures, which hinder conventional thermodynamic parametrization. While recent experimental developments have enabled the acquisition of measurable vapor pressure data for these systems [75,76], such data remain limited and are not incorporated in the current analysis, given their preliminary nature.

The parameter estimation procedure is initiated by gathering density measurements for the target DESs (Table 3). Estimates for m, σ, and ε are then derived through an optimization process, wherein an objective function is defined to quantify the deviation between the experimentally measured densities and those predicted by the SAFT model in *Clapeyron.jl* thermodynamic toolkit [46]. In this work, a least-square minimization approach is employed:

$$\text{Minimize} \quad \sum_{k}^{N_{\text{dp}}}\left(\frac{\rho_k^{\text{SAFT}}(T_k, P_k; m, \sigma, \varepsilon) - \rho_k^{\text{exp}}}{\rho_k^{\text{exp}}}\right)^2 \tag{16}$$

where ρ_k represents the k-th DES density at temperature T_k and pressure P_k, with SAFT and exp superscripts expressing the calculated and experimental values (Table 3), respectively. The Evolutionary Centers Algorithm optimization method [77] within the *Metaheuristic.jl* package [78] in Julia programming language [79] is utilized to adjust the parameters until the model output aligns optimally with the experimental data.

As detailed in the Theory section, the interaction energy between CO_2 and DES (ε_{ij}) can either be estimated using combining rules or treated as an adjustable parameter, optimized against experimental phase equilibrium data. The pure segment energy (ε) is conceptually associated with the interaction strength between molecular segments and is directly related to thermodynamic properties such as vapor pressure and heat capacity. Consequently, there are concerns regarding the reliability of combining rules to accurately predict ε_{ij} when the pure-component parameters are derived solely from density data. To mitigate this, a stepwise approach to parameter estimation is adopted. The pure-component parameters, obtained from Eq. (16) through fitting exclusively to density data, are retained. Subsequently, the CO_2–DES experimental phase equilibrium data (Table 4) is utilized to optimize a temperature-independent interaction energy parameter, ε_{ij}^{fit}, by minimizing the objective function specified in Eq. (17). This parameter is not fitted to each individual temperature to improve its transferability across different conditions and to enable a direct comparison with the interaction energy predicted using the combining rules (Eqs. (10) and 11).

$$\text{Minimize} \quad \sum_{k}^{N_{\text{dp}}}\left(\frac{P_k^{\text{SAFT}}(T_k, x_k; \varepsilon_{ij}) - P_k^{\text{exp}}}{P_k^{\text{exp}}}\right)^2 \tag{17}$$

where P_k represents the k-th CO_2–DES equilibrium pressure at temperature T_k and composition x_k.

Table 3
Experimental DES pure specific density data extracted from the corresponding literature (Ref. [68–70]).

Abbreviation	DES species	M_w (g/mol)	Pressure (MPa)	Temperature (K)	Density (kg/m^3)	N_{dp}	Ref.
des01	[Ch][Cl]:EG (1:2)	135.42	0.1–50.0	298.15–323.15	1103.0–1132.4	66	[68]
des02	[TPPP][Br]:Ph (1:6)	151.95	0.1	293.15–333.15	1129.1–1158.2	5	[69]
des03	[TPBP][Br]:Ph (1:4)	171.36	0.1	293.15–333.15	1045.7–1073.4	5	[69]
des04	[TPPP][Br]:Ph (1:4)	196.80	0.1	293.15–333.15	1144.3–1173.0	5	[69]
des05	[TBA][Cl]:CA (1:2)	207.48	0.1	288.15–323.15	901.0–923.2	8	[70]
des06	[MTA][Cl]:CA (1:2)	243.56	0.1	288.15–323.15	880.7–902.7	8	[70]
des07	[MTA][Br]:CA (1:2)	264.37	0.1	288.15–323.15	925.8–948.9	8	[70]
des08	[TOA][Cl]:CA (1:2)	282.29	0.1	288.15–323.15	873.2–895.3	8	[70]
des09	[TOA][Br]:CA (1:2)	297.11	0.1	288.15–323.15	913.6–936.4	8	[70]
des10	[TOA][Cl]:CA (1:1.5)	304.30	0.1	288.15–323.15	872.5–894.4	8	[70]
Total						*129*	

Table 4
Experimental CO_2–DES phase equilibria data extracted from the corresponding literature (Ref. [69–71]).

CO_2 system	Pressure (MPa)	Temperature (K)	CO_2 mole fraction	N_{dp}	Ref.
[Ch][Cl]:EG (1:2)	0.25–6.17	313.15–333.15	0.020–0.408	24	[71]
[TPPP][Br]: Ph (1:6)	0.16–1.39	313.15–333.15	0.021–0.195	18	[69]
[TPBP][Br]: Ph (1:4)	0.16–1.58	313.15–333.15	0.018–0.205	18	[69]
[TPPP][Br]: Ph (1:4)	0.18–1.35	313.15–333.15	0.020–0.213	18	[69]
[TBA][Cl]: CA (1:2)	0.09–1.99	298.15–323.15	0.009–0.239	36	[70]
[MTA][Cl]: CA (1:2)	0.09–1.99	298.15–308.15	0.011–0.252	18	[70]
[MTA][Br]: CA (1:2)	0.09–1.99	298.15–323.15	0.011–0.257	27	[70]
[TOA][Cl]: CA (1:2)	0.09–1.99	298.15–323.15	0.012–0.284	36	[70]
[TOA][Br]: CA (1:2)	0.09–1.99	298.15–323.15	0.011–0.283	27	[70]
[TOA][Cl]: CA (1:1.5)	0.09–1.99	298.15–323.15	0.012–0.299	33	[70]
Total				*255*	

The role of the combining rule and its impact on parameter sensitivity and model reliability will be discussed in detail in the Results and Discussion section, where we assess the robustness of the chosen parameters and the predictive capacity of the model.

It is worth mentioning that these optimized parameters are specific to each association scheme and cannot be transferred between them, requiring independent fitting. Table 5 presents the pure segment parameters (m, σ, and ε) for both PC-SAFT and SAFT-VR Mie DESs. The association energy and volume were set *a priori* for PC-SAFT (1000 K and 0.1) and SAFT-VR Mie (600 K and 1200 Å^3) across both association schemes. Additionally, the potential parameters (λ_r and λ_a) of SAFT-VR Mie were set to 16 and 6, respectively, for all DESs. In previous studies of ionic liquids [80,81], the association parameters $\varepsilon_{AB} = 5000$ K and $\kappa_{AB} = 0.1$ were employed under the assumption that strong intermolecular associations effectively constrains molecules or ions into structured aggregates, thereby replicating the negligible vapor pressures characteristic of ionic liquids. Molecular dynamics simulations support this assumption, indicating that ionic liquids exhibit pronounced self-association due to a combination of Coulombic interactions and hydrogen bonding, which leads to the formation of relatively rigid ionic networks [82–84]. In contrast, DESs predominantly rely on hydrogen bonding between constituent species, resulting in more transient and flexible molecular clusters [85]. Hence, a reduced association energy parameter is adopted for DESs to mitigate overfitting and maintain the physical plausibility of association parameters across a broad range of DES systems.

As shown in Table 5, the pure parameter estimation %AARD were below 1 %. The only parametrization conducted beyond 0.1 MPa was for [Ch][Cl]:EG (1:2) (des01), with %AARD ranging from 0.43 % to 0.76 %. The parameters for CO_2 were obtained from the literature and are presented in Table 6. For PC-SAFT, two approaches were considered for the CO_2–DES pair: treating CO_2 as an inert compound [26] or assuming a 2B cross-association with DES [81]. In the case of SAFT-VR Mie, CO_2 was modeled exclusively as an inert compound [25].

3.3. Association contribution to residual pressure

Molecular simulation studies have consistently revealed the presence of hydrogen-bonding networks in DES, highlighting the significant association among constituent molecules and its potential impact on their thermodynamic behavior [1,69,85–87].

Within the framework of SAFT, accurately capturing association effects is critical for predictive reliability. However, when DESs are modeled as pseudo-pure compounds, uncertainty arises regarding the extent to which these strong hydrogen-bonding interactions are represented. Specifically, it remains unclear how such interactions influence the prediction of thermodynamic properties and phase equilibria when the complex multi-component nature of DES is simplified into a single pseudo-pure entity.

Furthermore, the current methodology for pure-component parameter estimation relies on density data. Although density is a fundamental property, its exclusive use may not adequately account for the contributions of molecular association, particularly the influence of hydrogen bonding on residual pressure. Since residual pressure encapsulates deviations from ideal behavior, a rigorous quantification of the association contribution is essential. The contribution of association to residual pressure can be determined using the following expression:

$$\%p_{assoc} = 100\frac{|p_{assoc}|}{|p_{HS}| + |p_{disp}| + |p_{chain}| + |p_{assoc}|} \tag{18}$$

where p_{HS}, p_{disp}, p_{chain}, and p_{assoc} represent the pressure based on hard-sphere, dispersion, chain, and association contributions to the residual Helmholtz energy, respectively.

4. Results and discussion

4.1. CO_2–DES phase equilibria

In this section, we examine the performance of PC-SAFT and SAFT-VR Mie in predicting the solubility of CO_2 in the DESs presented in Table 4. The impact of different unlike-segment interaction energies (ε_{ij}), determined either via combining rules or empirical fitting, is also evaluated. Initially, no cross-association between CO_2 and DES is assumed, with cross-association effects evaluated at the end of the section. The empirical and calculated ε_{ij} values, along with the corresponding solubility %AARD for PC-SAFT and SAFT-VR Mie, are presented in Table 7 and Table 8, respectively.

Table 5
Pure parameters and density %AARD for the investigated DESs (Table 3). For PC-SAFT, $\varepsilon_{AB} = 1000$ K, and $\kappa_{AB} = 0.1$. For SAFT-VR Mie, $\varepsilon_{AB} = 600$ K, $K_{AB} = 1200$ Å^3, $\lambda_r = 16$, and $\lambda_a = 6$.

	des01	des02	des03	des04	des05	des06	des07	des08	des09	des10	*Avg.*
PC-SAFT (non-associating)											
m	5.9966	5.4904	4.6874	5.5759	3.3366	3.4033	3.4341	3.7716	3.8719	3.9728	
σ (Å)	2.5966	3.0623	3.4299	3.1551	4.6943	4.9592	4.9922	5.0288	4.9946	5.0670	
ε (K)	230	245	300	245	450	450	442	413	409	404	
%AARD	0.43	0.38	0.26	0.47	0.03	0.01	0.02	0.04	0.05	0.05	*0.17*
SAFT-VR Mie (non-associating)											
m	4.5375	5.5998	5.4404	6.2911	2.2600	2.7723	2.8999	3.5948	3.6694	3.9949	
σ (Å)	2.8977	3.0725	3.2954	3.0626	5.2974	5.2792	5.2608	5.1188	5.0954	5.0749	
ε (K)	315	300	347	300	425	425	425	425	425	425	
%AARD	0.49	0.62	0.39	0.71	0.22	0.14	0.13	0.07	0.07	0.06	*0.29*
PC-SAFT (2B association scheme)											
m	5.4957	5.1811	4.8970	5.4979	3.3180	3.3362	3.3638	3.8423	4.0948	4.0953	
σ (Å)	2.6834	3.1065	3.3705	3.1547	4.7063	4.9937	5.0344	4.9903	4.9011	5.0072	
ε (K)	227	220	268	220	414	414	414	371	371	362	
%AARD	0.46	0.52	0.35	0.62	0.06	0.05	0.05	0.08	0.09	0.10	*0.24*
SAFT-VR Mie (2B association scheme)											
m	4.4984	5.3465	5.7309	5.7733	2.6357	2.9759	3.0987	3.8229	3.8817	4.3873	
σ (Å)	2.9067	3.0971	3.2197	3.1252	5.0526	5.1641	5.1531	5.0170	5.0029	4.9205	
ε (K)	299	274	316	274	413	413	413	413	413	413	
%AARD	0.51	0.81	0.52	0.92	0.17	0.13	0.12	0.07	0.08	0.06	*0.34*
PC-SAFT (4C association scheme)											
m	4.5600	5.3990	5.3838	5.4992	3.2002	3.3382	3.3523	3.6457	3.8619	4.1006	
σ (Å)	2.8675	3.0509	3.2360	3.1278	4.7110	4.9378	4.9834	5.0185	4.9335	4.9516	
ε (K)	210	186	214	181	303	303	303	276	276	276	
%AARD	0.54	0.65	0.48	0.85	0.10	0.09	0.10	0.13	0.15	0.15	*0.32*
SAFT-VR Mie (4C association scheme)											
m	4.8976	5.3992	5.7102	5.9926	3.4836	3.7787	3.8155	4.4023	4.5242	4.8982	
σ (Å)	2.7812	3.0787	3.2025	3.0755	4.6319	4.7915	4.8273	4.7985	4.7652	4.7511	
ε (K)	238	250	281	250	402	402	402	402	402	402	
%AARD	0.76	0.85	0.64	0.99	0.07	0.05	0.06	0.04	0.05	0.04	*0.36*

Table 6
CO_2 pure parameters extracted from literature (Ref. [25,26,81]).

CO_2 model	m	σ (Å)	ε (K)	$\varepsilon_{A_iB_j}$ (K)	$\kappa_{A_iB_j}$	λ_r	λ_a	Ref.
PC-SAFT (inert)	2.0729	2.7852	169.21					[26]
PC-SAFT (2B)	2.0729	2.7852	169.21	0	0.1			[81]
SAFT-VR Mie (inert)	1.6936	3.0465	235.73			18.067	6	[25]

Table 7
PC-SAFT %AARD of CO_2(inert)–DES phase equilibria using ε_{ij} from solubility data or combining rules (Eqs. (10) and 11) and the corresponding k_{ij} (Eq. (12)).

	des01	des02	des03	des04	*Avg.*	des05	des06	des07	des08	des09	des10	*Avg.*
PC-SAFT (non-associating)												
ε_{ij}^{fit} (K)	196.7897	201.4590	217.6457	201.1097		222.9581	214.2621	210.9693	203.8852	204.1256	201.6604	
ε_{ij}^{HM} (K)	196.5513	202.2400	218.1114	201.2493		225.4476	215.7131	212.5899	204.2160	204.4162	200.6584	
ε_{ij}^{LB} (K)	197.2772	203.6086	225.3065	203.6086		275.9429	275.9429	273.4791	264.3553	263.0720	261.4591	
k_{ij}^{HM}	−0.0012	0.0039	0.0021	0.0007		0.0110	0.0067	0.0076	0.0016	0.0014	−0.0050	
k_{ij}^{LB}	0.0025	0.0106	0.0340	0.0123		0.1920	0.2235	0.2286	0.2287	0.2241	0.2287	
%AARD^{fit}	8.73	5.11	7.20	7.73	*7.19*	3.25	2.24	2.74	3.30	3.44	3.97	*3.16*
%AARD^{HM}	8.81	6.16	7.97	7.94	*7.72*	9.81	5.74	6.63	3.49	3.63	4.71	*5.67*
%AARD^{LB}	9.13	11.7	35.3	15.9	*18.0*	89.0	91.6	91.2	90.1	89.8	89.6	*90.2*
PC-SAFT (2B association scheme)												
ε_{ij}^{fit} (K)	196.2356	190.0974	207.2169	190.6014		215.5066	206.1867	205.1774	195.4437	198.5877	193.5280	
ε_{ij}^{HM} (K)	195.7827	191.2246	207.2277	190.7097		215.8184	205.6935	204.2670	194.8315	197.7998	191.8995	
ε_{ij}^{LB} (K)	195.9864	192.9409	212.9514	192.9409		264.6752	264.6752	264.6752	250.5532	250.5532	247.4955	
k_{ij}^{HM}	−0.0023	0.0059	0.0001	0.0006		0.0014	−0.0024	−0.0045	−0.0031	−0.0040	−0.0085	
k_{ij}^{LB}	−0.0013	0.0147	0.0269	0.0121		0.1858	0.2210	0.2248	0.2200	0.2074	0.2181	
%AARD^{fit}	8.90	5.25	7.30	7.69	*7.28*	3.26	2.07	2.63	3.25	3.47	3.85	*3.09*
%AARD^{HM}	9.08	6.98	7.30	7.71	*7.77*	3.44	2.88	3.97	3.94	4.15	6.16	*4.09*
%AARD^{LB}	8.98	14.4	28.5	14.2	*16.5*	87.1	90.2	90.0	87.8	87.1	87.2	*88.2*
PC-SAFT (4C association scheme)												
ε_{ij}^{fit} (K)	189.2801	177.4458	187.1426	174.8520		184.9938	178.3987	177.4428	169.0546	170.1905	170.4409	
ε_{ij}^{HM} (K)	188.3851	176.3056	187.1097	173.2491		184.4913	177.6510	176.2804	167.2380	169.6747	169.1551	
ε_{ij}^{LB} (K)	188.5049	177.4065	190.2917	175.0057		226.4302	226.4302	226.4302	216.1064	216.1064	216.1064	
k_{ij}^{HM}	−0.0048	−0.0065	−0.0002	−0.0093		−0.0027	−0.0042	−0.0066	−0.0109	−0.0030	−0.0076	
k_{ij}^{LB}	−0.0041	−0.0002	0.0165	0.0009		0.1830	0.2121	0.2163	0.2177	0.2125	0.2113	
%AARD^{fit}	8.31	5.28	7.50	7.38	*7.12*	3.17	1.80	2.49	3.02	3.14	3.44	*2.84*
%AARD^{HM}	9.32	7.72	7.51	9.67	*8.56*	3.46	3.92	4.56	5.78	3.49	5.16	*4.40*
%AARD^{LB}	9.04	5.30	17.7	7.42	*9.86*	81.1	84.4	84.2	82.2	82.0	81.6	*82.6*

Table 8
SAFT-VR Mie %AARD of CO_2(inert)–DES phase equilibria using ε_{ij} from solubility data or combining rules and the corresponding k_{ij}.

	des01	des02	des03	des04	*Avg.*	des05	des06	des07	des08	des09	des10	*Avg.*
SAFT-VR Mie (non-associating)												
ε_{ij}^{fit} (K)	271.6729	265.5781	284.3027	267.1465		250.4036	250.5604	251.6989	257.9416	257.9210	259.9357	
ε_{ij}^{HM} (K)	271.9857	265.9160	284.6845	265.9249		252.3244	253.0260	253.7356	259.2131	260.1152	260.9050	
ε_{ij}^{LB} (K)	272.4976	265.9304	286.0040	265.9304		316.5205	316.5205	316.5205	316.5205	316.5205	316.5205	
k_{ij}^{HM}	0.0011	0.0013	0.0013	−0.0046		0.0076	0.0097	0.0080	0.0049	0.0084	0.0037	
k_{ij}^{LB}	0.0030	0.0013	0.0059	−0.0046		0.2089	0.2084	0.2048	0.1851	0.1851	0.1788	
%AARD^{fit}	7.84	5.10	8.38	8.54	*7.47*	3.04	4.35	4.39	3.42	3.37	3.57	*3.69*
%AARD^{HM}	7.98	5.36	8.58	9.78	*7.93*	5.31	7.26	6.43	4.66	6.87	4.11	*5.77*
%AARD^{LB}	8.51	5.37	11.28	9.77	*8.73*	84.22	85.49	84.60	82.81	83.03	82.08	*83.71*
SAFT-VR Mie (2B association scheme)												
ε_{ij}^{fit} (K)	266.1193	252.5099	271.5035	253.2248		257.4533	253.5791	254.1485	258.9832	258.9150	261.8842	
ε_{ij}^{HM} (K)	265.0479	254.0940	272.3047	254.0217		258.0419	253.8052	254.2235	259.3921	259.9264	263.0418	
ε_{ij}^{LB} (K)	265.4869	254.1457	272.9298	254.1457		312.0200	312.0200	312.0200	312.0200	312.0200	312.0200	
k_{ij}^{HM}	−0.0040	0.0062	0.0029	0.0031		0.0023	0.0009	0.0003	0.0016	0.0039	0.0044	
k_{ij}^{LB}	−0.0024	0.0064	0.0052	0.0036		0.1749	0.1873	0.1855	0.1700	0.1702	0.1607	
%AARD^{fit}	7.54	5.15	8.20	8.18	*7.27*	2.04	3.55	3.89	2.91	2.92	3.07	*3.06*
%AARD^{HM}	8.51	7.57	9.28	8.99	*8.59*	2.40	3.63	3.89	2.98	4.12	4.56	*3.60*
%AARD^{LB}	7.81	7.71	10.71	9.21	*8.86*	80.48	82.91	82.05	80.39	80.68	79.46	*81.00*
SAFT-VR Mie (4C association scheme)												
ε_{ij}^{fit} (K)	235.9950	244.0628	256.4025	244.3816		269.2284	262.8287	262.5377	264.1727	264.1615	265.0366	
ε_{ij}^{HM} (K)	235.3927	242.7400	256.8907	242.7438		270.1202	264.2938	262.9726	264.0358	265.2614	265.7791	
ε_{ij}^{LB} (K)	236.8623	242.7602	257.3716	242.7602		307.8367	307.8367	307.8367	307.8367	307.8367	307.8367	
k_{ij}^{HM}	−0.0026	−0.0054	0.0019	−0.0067		0.0033	0.0055	0.0017	−0.0005	0.0041	0.0028	
k_{ij}^{LB}	0.0037	−0.0054	0.0038	−0.0067		0.1254	0.1462	0.1472	0.1418	0.1419	0.1390	
%AARD^{fit}	7.87	5.14	8.10	8.31	*7.36*	1.64	2.71	3.84	2.77	2.88	2.90	*2.79*
%AARD^{HM}	8.31	7.08	8.57	9.97	*8.48*	3.05	4.59	4.01	2.79	3.99	3.10	*3.59*
%AARD^{LB}	8.49	7.02	9.56	9.95	*8.76*	72.95	77.55	76.88	76.03	76.25	75.52	*75.86*

Table 7 and Table 8 are not suited for exhaustive analysis but provide a useful starting point. The DESs have been divided into two groups: des01–des04 represent the hydrophilic group, while des05–des10 represent the CA-based DESs, which are hydrophobic.

It is acknowledged that water content – which can be explicitly modeled in the CO_2–DES mixture, as demonstrated by Cea-Klapp et al. [39] with a 2 % water inclusion – affects the predictions. One complication arises because the 'pure' parameters inherently include water in their formulation. Therefore, parameter estimation should either rigorously separate the DES into a water–DES mixture and perform parameterization using water parameters, or, as adopted in this work, a simpler approach should be used that assumes the 'pure' parameters already account for the water content. This assumption implies that the water content does not significantly affect predictions within the equilibrium pressure range.

The rigorous approach increases modeling complexity and requires careful scrutiny of the water parameters, which themselves possess uncertainties and may necessitate unique parametrization for the CO_2–water–DES ternary mixture. While other authors have examined the impact of water in such models [39,88,89], the simpler description also allows for a more straightforward comparison of equations of state and combining rules, as the rigorous approach increases the degrees of freedom associated with the water model. This methodology is also consistent with the modeling of hydrophobic DESs.

A particularly noteworthy result across both equations of state and all association strategies is the prediction of CO_2 solubility in hydrophobic DESs (des05–des10) using the Lorentz-Berthelot (LB) combining rule (Eq. (10)), which yielded an average %AARD exceeding 75 %. The

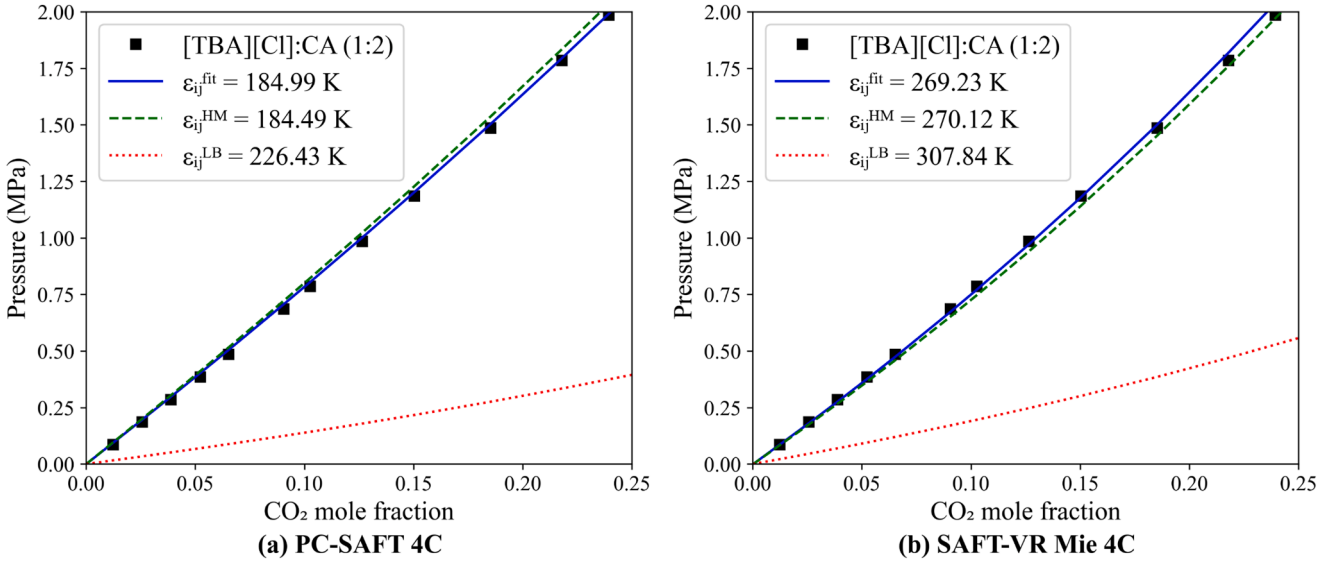

Fig. 1. CO_2–DES phase equilibria of [TBA][Cl]:CA (1:2) (des05) at 298.15 K with different ε_{ij} approaches for (a) PC-SAFT 4C and (b) SAFT-VR Mie 4C models. Symbols represent experimental data [70] (Table 4), while the lines are the SAFT calculations.

qualitative trends for all hydrophobic DESs align with Fig. 1, where both PC-SAFT and SAFT-VR Mie with LB significantly underpredict the equilibrium pressure due to an overestimation of the attractive interaction (indicated by a positive k_{ij}). By incorporating the size parameter σ, the Hudson-McCoubrey (HM) rule (Eq. (11)) accounts for the volumetric contribution of the interacting particles, offering a more physically realistic representation of how dispersion forces scale with molecular size [28]. Since larger molecules exhibit stronger cumulative dispersion forces, the HM rule adjusts the interaction energy accordingly. In contrast, the LB rule assumes uniform interaction strength between the pure component potential depths – a simplification that does not hold for the CO_2–DES system, where substantial asymmetries exist. Given the challenges of relying solely on density for estimating ε, these findings suggest that models incorporating the HM rule may more accurately predict the energetic balance of the CO_2–DES interactions than those utilizing LB rules. By integrating σ, the HM rule mitigates the limitations of pure segment energy ε.

For hydrophilic DESs (des01–des04), the choice of combining rule exerts a reduced influence on the SAFT-VR Mie modeling results. This behavior is primarily attributed to the 'volume ratio' between CO_2 and the DES segments, which appears as a multiplicative factor in the interaction energy expression within the HM combining rule (Eq. (11)). For des01–des04, this volume ratio is approximately 1.0, thereby minimizing its effect on the predicted ε_{ij} values. In contrast, for des05–des10, the volume ratio decreases to approximately 0.91, leading to a more significant impact of ε_{ij} and, consequently, a greater influence on the overall modeling predictions. Nevertheless, we recommend avoiding the LB rule for DES mixtures, due to the vast number of possible compounds and the absence of any computational performance trade-offs when employing alternative unlike-segment interaction energy strategies.

Another significant finding is the prediction for [Ch][Cl]:EG (1:2) (des01), the only DES for which pure parameter estimation used a pressure range beyond 0.1 MPa (0.1 MPa to 50 MPa). The %AARD for des01 ranges from 7.54 % and 8.51 %, comparable to the average % AARD of the hydrophilic group. As illustrated in Fig. 2, results from both fitted and predicted ε_{ij} are closely aligned, highlighting the model's ability to extend solubility predictions beyond the 0.1 MPa density used for parameter estimation in des02–des10. This demonstrates that PC-SAFT and SAFT-VR Mie can accurately predict CO_2–DES equilibrium pressures beyond the pure parametrization range. Chapman et al. [90] demonstrated that by decomposing the Helmholtz free energy into distinct contributions – such as repulsive, dispersive, chain, and association terms – the SAFT framework employs physically meaningful parameters (e.g., segment diameter, dispersion energy, and association parameters) that remain valid across a broad range of conditions, even when derived at a single pressure level (e.g., 0.1 MPa). Building upon these principles, Gross and Sadowski (2001) [26] extended the approach in developing the PC-SAFT model, further reinforcing that the statistical-mechanical foundation of SAFT effectively accounts for pressure-dependent behavior. As a result, these models can reliably predict phase equilibria, provided that they are supported by a rigorous parameterization procedure and well-defined modeling strategies.

Figs. 3–8 provide a clearer illustration of the overall results presented in Table 7 and Table 8. Fig. 3 and Fig. 4 depict the performance of PC-SAFT for various association and unlike-segment interaction energy strategies applied to des01–des04 and des05–des10, respectively. Since solubility predictions depend on both pure-component parameters and interaction parameters, each association strategy yields different results.

As shown in Fig. 3, PC-SAFT using the HM rule yielded comparable results for the NA (%AARD = 7.72 %) and 2B strategies (%AARD = 7.77 %), while the 4C strategy resulted in a slightly higher %AARD of 8.56 %. These values are similar to those obtained when PC-SAFT was fitted to solubility data, where %AARD ranged from 7.12 % to 7.28 %. In contrast, the PC-SAFT based on the LB rule was ineffective in accurately predicting solubility for these systems. It is noteworthy that the 4C association scheme reduced the %AARD to 9.86 %, compared to 18.0 % for the non-associating approach and 16.5 % for the 2B scheme. This improvement is likely due to the stronger association compensating for interaction energies not captured by the Lorentz-Berthelot combining rule.

For des05–des10 (Fig. 4), among the association strategies, the 2B PC-SAFT approach provided the most accurate predictions, with a % AARD of 4.09 %. This is approximately 1 % higher than the %AARD obtained with ε_{ij}^{fit} (3.09 %) but about 1.5 % lower than the predictive NA PC-SAFT model (5.67 %).

As previously discussed, for the modeling of des01–des04 using SAFT-VR Mie (Fig. 5), the LB rule performs comparably to the HM rule. Nevertheless, between the two, the HM rule yields better results, with the lowest %AARD (7.93 %) observed for the NA strategy. This is about 0.5 % higher than the average %AARD of 7.47 % obtained using ε_{ij}^{fit} for the same strategy. The SAFT-VR Mie model based on the HM rule

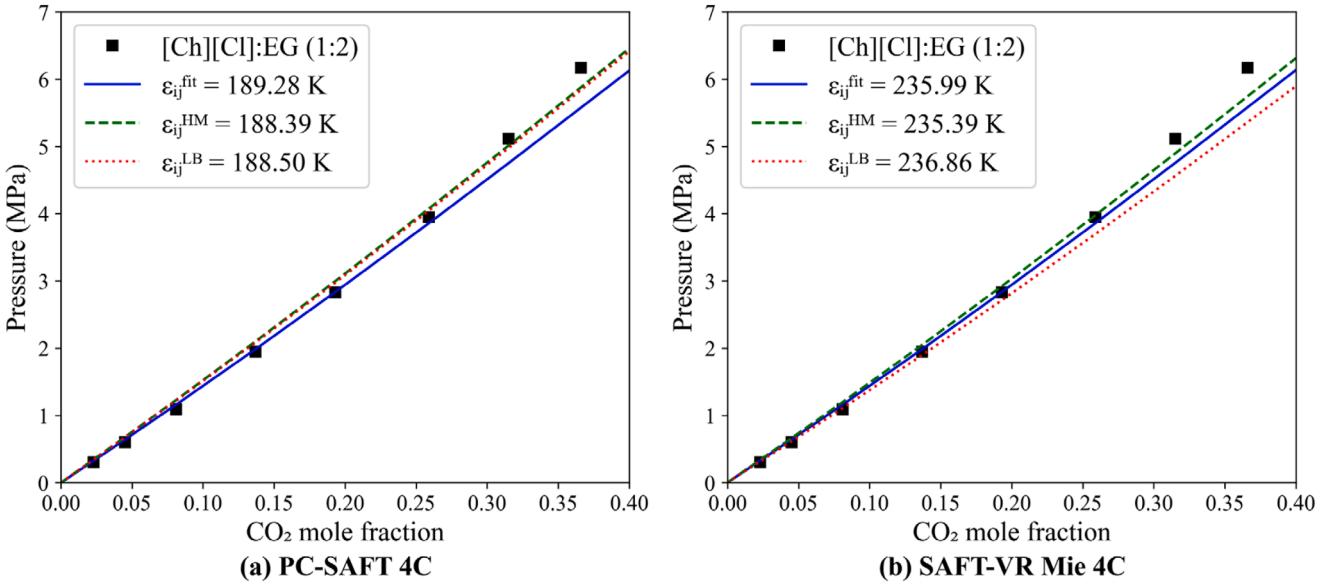

Fig. 2. CO_2–DES phase equilibria of [Ch][Cl]:EG (1:2) (des01) at 323.15 K with different ε_{ij} approaches for (a) PC-SAFT 4C and (b) SAFT-VR Mie 4C models (lines). Symbols represent experimental data [71] (Table 4), while the lines are the SAFT calculations.

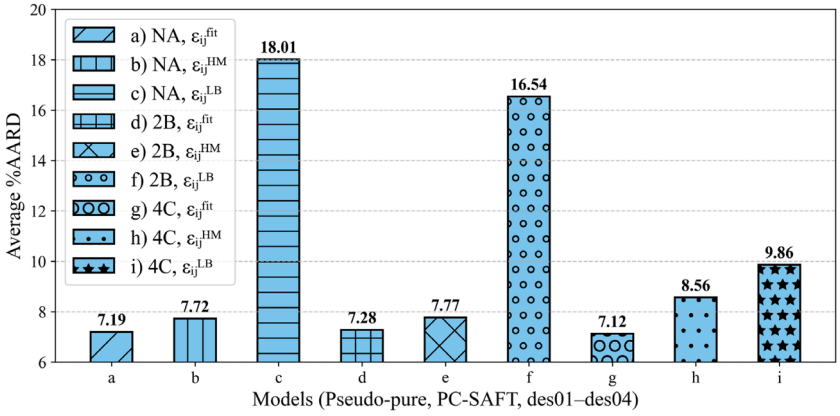

Fig. 3. Average %AARD of CO_2 solubility in hydrophilic DESs (des01–des04) using PC-SAFT with various unlike-segment energy and association strategies.

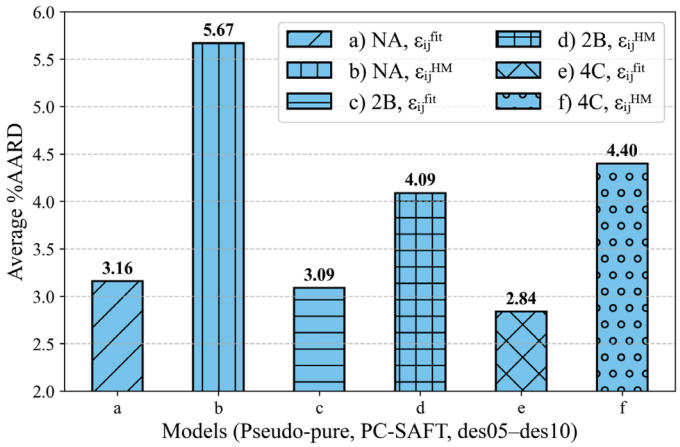

Fig. 4. Average %AARD of CO_2 solubility in hydrophobic DESs (des05–des10) using PC-SAFT with various unlike-segment energy and association strategies.

remains effective using self-association, yielding %AARD values of 8.59 % and 8.48 % for the 2B and 4C association schemes, respectively.

The marginally better performance of the non-associating description in some modeling strategies can be explained by several factors [31,35,42,91]. First, by treating the DES as a pseudo-pure component, the model effectively captures the overall hydrogen bonding effects through the fitted SAFT parameters, such as dispersion and chain parameters. This "averaging" effect allows the model to account for hydrogen bonding without explicitly incorporating self-association. Second, introducing self-association into the model requires additional parameters, such as association energy and volume, which cannot be reliably estimated from density data alone. Poorly constrained association parameters may lead to numerical instabilities or compensation effects that degrade overall model performance. Finally, the microstructure of DESs is inherently heterogeneous and dynamic. Many self-association thermodynamic models rely on static assumptions that may not fully capture the transient and fluctuating nature of hydrogen bonds in DESs, whereas molecular dynamics simulations can provide a more accurate representation of these interactions.

For des05–des10, the 2B and 4C strategies yielded %AARD values of approximately 3.6 % when SAFT-VR Mie was applied with the HM rule (Fig. 6). Interestingly, for the NA strategy, the results were inferior to those assuming self-association, even with ε_{ij}^{fit}. This suggests that these systems are better represented with self-association.

Since the HM rule outperforms the LB rule, we compare the predictive capabilities of PC-SAFT and SAFT-VR Mie EoS, both implemented with the HM rule. Fig. 7 and Fig. 8 present the average %AARD for des01–des04 and des05–des10, respectively. For hydrophilic DESs (Fig. 7), PC-SAFT and SAFT-VR Mie exhibit comparable performance, with a margin of difference within 0.3 % for the NA strategy. In contrast, for hydrophobic DESs (Fig. 8), SAFT-VR Mie outperforms PC-SAFT, resulting in a 0.5 % improvement in the 2B scheme and a 0.8 % improvement in the 4C scheme, while the NA strategy demonstrates lower effectiveness.

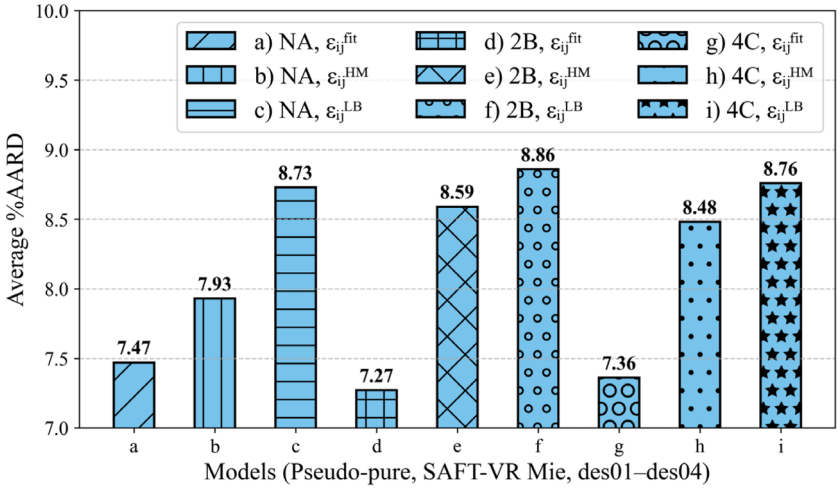

Fig. 5. Average %AARD of CO_2 solubility in hydrophilic DESs (des01–des04) using SAFT-VR Mie with various unlike-segment energy and association strategies.

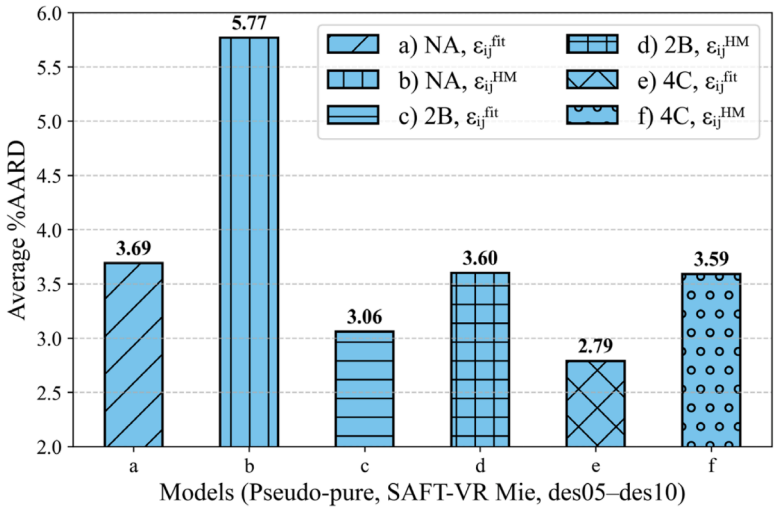

Fig. 6. Average %AARD of CO_2 solubility in hydrophobic DESs (des05–des10) using SAFT-VR Mie with various unlike-segment energy and association strategies.

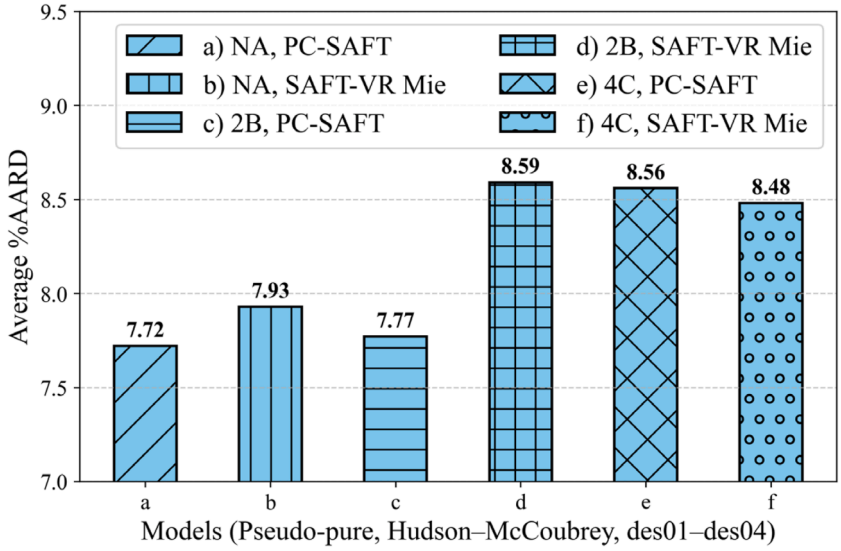

Fig. 7. Average %AARD of CO_2 solubility in hydrophilic DESs (des01–des04) for various models based on the Hudson-McCoubrey combining rule.

Moreover, the average %AARD of hydrophobic DESs (Fig. 8) is approximately half of that of the hydrophilic compounds (Fig. 7). This discrepancy may be attributed to errors arising from the constrained modeling of water in these compounds, which, in turn, complicates the comparison between the PC-SAFT and SAFT-VR Mie models.

The exceptional performance of the SAFT-VR Mie for des05–des10 was achieved by modeling DESs with a repulsive exponent (λ_r) of 16, rather than the conventional value of 12. This adjustment provided a more accurate representation of phase equilibria and improved numerical stability. A molecular simulation study [85] on the interaction mechanism of CO_2 with hydrophobic DES systems suggested that absorbed CO_2 reduces the cluster size of hydrophobic DES component by occupying liquid voids. This process preserves hydrogen bonding while impeding long-range interactions. Hence, a steeper repulsive wall more effectively captures the 'hard-core' behavior of molecules. Since local structure and molecular packing are critical in DESs, this modification emphasizes the representation of solvent exclusion at short distances. From a practical modeling perspective, the chosen λ_r of 16 aligns more closely with that of CO_2 ($\lambda_r = 18.067$), thereby reducing the reliance on combining rules. In this work, we employed the combining rules proposed in the original SAFT-VR Mie framework [24] for the exponent terms.

The results presented thus far were obtained under the assumption that CO_2 behaves as an inert component. Table 9 compares the average %AARD values for the CO_2–DES systems listed in Table 4, modeled using PC-SAFT with the HM combining rule. The comparison includes cases both without cross-association (i.e., treating CO_2 as inert) and with a 2B cross-association between CO_2 and the DESs. The negligible difference observed (only 0.01 % in some instances) indicates that cross-association has no meaningful impact on the results. Therefore, modeling efforts for these systems should focus on more influential factors, such as the choice of combining rules and association schemes.

4.2. *Contributions to the residual pressure*

In this section, we examine the contributions to the residual pressure (as defined in Eq. (18)) for hydrophobic DESs, which are free of water, thereby nullifying its influence on their parameterization. The association contribution to the residual pressure at 0.1 MPa and 298.15 K is illustrated in Fig. 9. Additionally, the first-order derivatives of each reduced Helmholtz energy contribution with respect to volume – evaluated at 298.15 K and constant particle number – are provided in Fig. 10

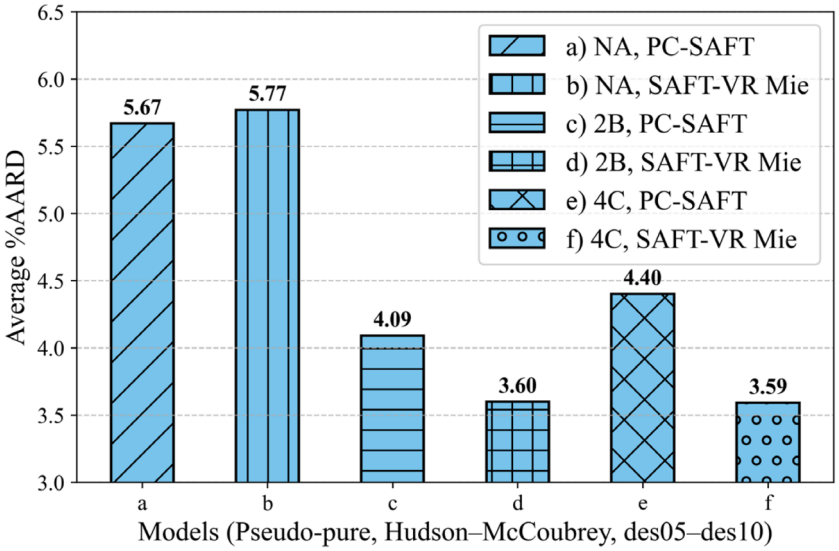

Fig. 8. Average %AARD of CO_2 solubility in hydrophobic DESs (des05–des10) for various models based on the Hudson-McCoubrey combining rule.

Table 9
PC-SAFT (HM rule) average %AARD of CO_2 solubility in DESs with and without CO_2–DES cross-association for various DES self-association strategies.

Models	NA	2B	4C	*Avg.*
CO_2(inert)–Hydrophilic DESs	7.72	7.77	8.56	*8.02*
CO_2(2B)–Hydrophilic DESs	7.71	7.77	8.57	*8.02*
CO_2(inert)–Hydrophobic DESs	5.67	4.09	4.40	*4.72*
CO_2(2B)–Hydrophobic DESs	5.66	4.10	4.40	*4.72*

for the [TBA][Cl]:CA (1:2) compound.

Although the association contribution to the residual pressure is relatively minor, ranging from 0.9 % in the 2B SAFT-VR Mie model (Fig. 9a) to 7.8 % in the 4C PC-SAFT model (Fig. 9b), it nevertheless enhances model performance (Fig. 8), as this contribution compensates for approximations in the SAFT NA model by balancing the overall interactions within the pseudo-pure approach.

Furthermore, the example in Fig. 10 demonstrates that the 'total' residual pressure pattern is predominantly governed by the hard-sphere term in both the PC-SAFT (Fig. 10a) and SAFT-VR Mie (Fig. 10b) models, while the association derivative remains essentially constant under the specified conditions. These findings are in agreement with previous studies on ionic liquids that employed the SAFT-VR Morse [92] and SAFT-VR Mie [93] EoS.

5. Conclusions

The challenge of accurately modeling the thermodynamic interactions between CO_2 and DESs has been the subject of extensive research, yet no consensus has been reached on the optimal predictive modeling approach. This study systematically investigates and compares the influence of four key factors that often vary across different modeling strategies: (i) the choice of the underlying thermodynamic framework, specifically PC-SAFT or SAFT-VR Mie equations of state; (ii) the method for determining the unlike-segment interaction energy between CO_2 and DES, whether through the Lorentz-Berthelot or Hudson-McCoubrey combining rules, or using experimental phase equilibrium data to adjust the parameter in the SAFT model; (iii) the treatment of

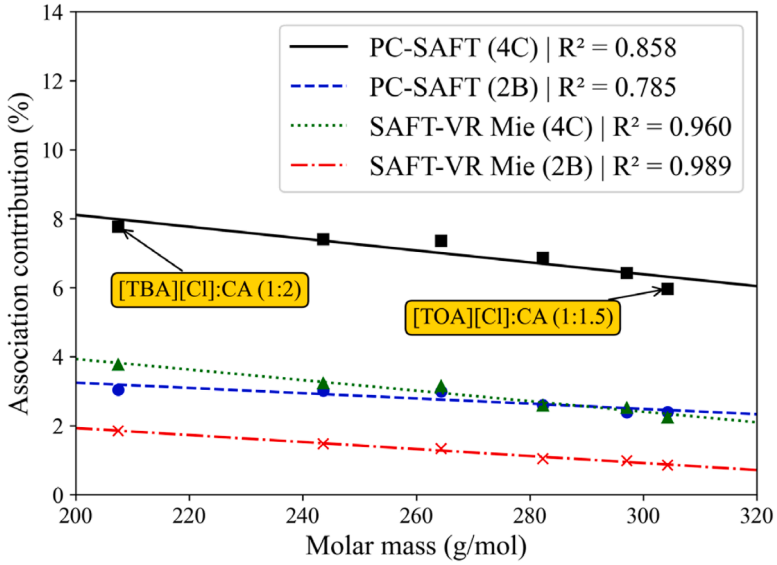

Fig. 9. Association contribution to the residual pressure at 0.1 MPa and 298.15 K. Symbols represent the SAFT calculations and lines are the linear fit using the least-squares method.

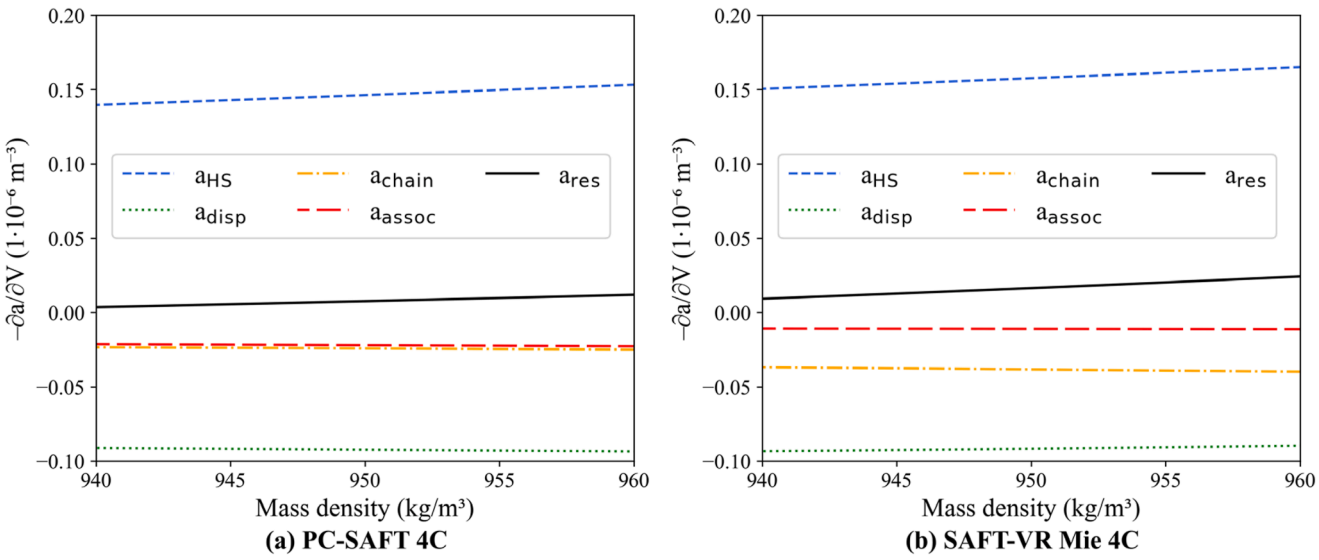

Fig. 10. Contributions to the reduced residual Helmholtz energy with respect to volume, at 298.15 K and 1.0 mol, for the [TBA][Cl]:CA (1:2) DES based on a) PC-SAFT, and b) SAFT-VR Mie 4C models.

hydrogen bonding within DES, considering it as either non-associating or as associating species following the 2B or 4C association schemes; and (iv) the representation of cross-association between CO_2 and DES, where CO_2 is modeled either as an inert compound or as an associating species interacting with DES.

Ten CO_2–DES phase equilibrium systems were analyzed, categorized into two groups: four hydrophilic DESs and six hydrophobic DESs. The modeling was conducted using the *Clapeyron.jl* open-source thermodynamic toolkit, employing the implemented SAFT variants and combining rule models. DESs were modeled as pseudo-pure components and treated either as non-associating species or as associating species, following the 2B or 4C association schemes in both PC-SAFT and SAFT-VR Mie frameworks.

Pure-component parameters (m, σ, and ε) for the DESs in the SAFT models were regressed against experimental density data. The unlike-segment interaction energy between CO_2 and DES was either estimated via combining rules or optimized to match experimental solubility data. The results demonstrate that the use of a simplified Hudson-McCoubrey combining rule yields phase equilibrium predictions comparable in accuracy to those obtained by optimization of the unlike-segment interaction energy using solubility measurements. In contrast, the Lorentz-Berthelot rule exhibited poor predictive capability – particularly for hydrophobic DESs – and should be avoided for CO_2–DES phase equilibria modeling.

For CO_2 solubility in hydrophilic DESs, modeling DESs as either non-associating species or using the 2B association scheme yielded comparable performance within the PC-SAFT framework. In the case of SAFT-VR Mie, hydrophilic DESs were best represented as non-associating species, although the 2B and 4C schemes remained within a 0.7 % deviation range, with both equations of state exhibiting similar predictive accuracy. For hydrophobic DESs, the 2B and 4C association schemes provided a more accurate representation, with SAFT-VR Mie exhibiting slightly superior accuracy. This improvement was achieved by adjusting the repulsive-attractive exponents of the SAFT-VR Mie DESs to 16–6 instead of modeling them as Lennard-Jones 12–6 species.

Moreover, cross-association between CO_2 and DESs had no significant impact on the CO_2–DES phase equilibria predictions. Finally, while association contributions to the residual pressure were minor, they positively influenced model performance, highlighting the role of hydrogen bonding in deep eutectic solvents.

CRediT authorship contribution statement

Cleiton S. Beraldo: Writing – original draft, Visualization, Validation, Methodology, Investigation, Formal analysis, Data curation, Conceptualization. **Luis A. Follegatti-Romero:** Writing – review & editing, Supervision, Resources, Project administration, Methodology, Funding acquisition. **Georgios M. Kontogeorgis:** Writing – review & editing, Visualization, Supervision, Methodology, Formal analysis, Conceptualization. **Xiaodong Liang:** Writing – review & editing, Visualization, Supervision, Software, Resources, Project administration, Methodology, Funding acquisition, Formal analysis, Conceptualization.

Declaration of competing interest

The authors declare that they have no known competing financial interests or personal relationships that could have appeared to influence the work reported in this paper.

Acknowledgement

This study was financed in part by the Coordenação de Aperfeiçoamento de Pessoal de Nível Superior (CAPES), Brazil – Finance Code 001, and the São Paulo Research Foundation (FAPESP), Brazil – Process Number 2024/10537–6. Luis A. Follegatti-Romero wishes to express his sincere gratitude for the support received from FAPESP under grant 2019/22085–4, as well as from Petronas (Petroliam Nasional Berhad) for Project No ANP 23708–1. Xiaodong Liang wants to thank the support from the Independent Research Fund Denmark (Case number: 3105–00024B).

Data availability

The scripts used for parameter estimation, density, solubility, and Helmholtz energy modeling are available on the following GitHub page: https://github.com/311cleiton/DES-Modeling.

References

[1] R. Stefanovic, M. Ludwig, G.B. Webber, R. Atkin, A.J. Page, Nanostructure, hydrogen bonding and rheology in choline chloride deep eutectic solvents as a function of the hydrogen bond donor, Phys. Chem. Chem. Phys 19 (2017) 3297–3306, https://doi.org/10.1039/c6cp07932f.

[2] Y. Zhang, X. Ji, X. Lu, Choline-based deep eutectic solvents for CO2 separation: review and thermodynamic analysis, Renew. Sustain. Energy Rev 97 (2018) 436–455, https://doi.org/10.1016/j.rser.2018.08.007.

[3] M. Ammar, S. Ashraf, D.A. Gonzalez-casamachin, D.T. Awotoye, J. Baltrusaitis, Recent progress of urea-based deep eutectic solvents as electrolytes in battery technology: a critical review, Batteries 10 (2024) 45, https://doi.org/10.3390/batteries10020045.

[4] J.I. García, H. García-Marín, E. Pires, Glycerol based solvents: synthesis, properties and applications, Green Chem 16 (2014) 1007–1033, https://doi.org/10.1039/C3GC41857J.

[5] Y. Wang, H. Liu, X. Ji, Q. Wang, Z. Tian, P. Fatehi, Production of nanocellulose using acidic deep eutectic solvents based on choline chloride and carboxylic acids: a review, Int. J. Biol. Macromol 245 (2023) 125227, https://doi.org/10.1016/j.ijbiomac.2023.125227.

[6] A. Krishnan, K.P. Gopinath, D.-V.N. Vo, R. Malolan, V.M. Nagarajan, J. Arun, Ionic liquids, deep eutectic solvents and liquid polymers as green solvents in carbon capture technologies: a review, Env. Chem. Lett 18 (2020) 2031–2054, https://doi.org/10.1007/s10311-020-01057-y.

[7] Q. Ren, AI in chemical engineering: a new chapter of innovation, Engineering 39 (2024) 1–2, https://doi.org/10.1016/j.eng.2024.07.006.

[8] A. Roda, A. Matias, A. Paiva, A. Duarte, Polymer science and engineering using deep eutectic solvents, Polym. (Basel) 11 (2019) 912, https://doi.org/10.3390/polym11050912.

[9] F. Oyoun, A. Toncheva, L.C. Henríquez, R. Grougnet, F. Laoutid, N. Mignet, K. Alhareth, Y. Corvis, Deep eutectic solvents: an eco-friendly design for drug engineering, ChemSusChem 16 (2023), https://doi.org/10.1002/cssc.202300669.

[10] F.P. Pelaquim, A.M. Barbosa Neto, I.A.L. Dalmolin, M.C. da Costa, Gas solubility using deep eutectic solvents: review and analysis, Ind. Eng. Chem. Res 60 (2021) 8607–8620, https://doi.org/10.1021/acs.iecr.1c00947.

[11] E.L. Smith, A.P. Abbott, K.S. Ryder, Deep eutectic solvents (DESs) and their applications, Chem. Rev 114 (2014) 11060–11082, https://doi.org/10.1021/cr300162p.

[12] A.E. Ünlü, A. Arıkaya, S. Takaç, Use of deep eutectic solvents as catalyst: a mini-review, Green Process. Synth 8 (2019) 355–372, https://doi.org/10.1515/gps-2019-0003.

[13] G. García, S. Aparicio, R. Ullah, M. Atilhan, Deep eutectic solvents: physicochemical properties and gas separation applications, Energy Fuels 29 (2015) 2616–2644, https://doi.org/10.1021/ef5028873.

[14] X. Li, K.H. Row, Development of deep eutectic solvents applied in extraction and separation, J. Sep. Sci 39 (2016) 3505–3520, https://doi.org/10.1002/jssc.201600633.

[15] Z. Yuan, H. Liu, W.F. Yong, Q. She, J. Esteban, Status and advances of deep eutectic solvents for metal separation and recovery, Green Chem 24 (2022) 1895–1929, https://doi.org/10.1039/D1GC03851F.

[16] F.M. Perna, P. Vitale, V. Capriati, Deep eutectic solvents and their applications as green solvents, Curr. Opin. Green Sustain. Chem 21 (2020) 27–33, https://doi.org/10.1016/j.cogsc.2019.09.004.

[17] J. Ruiz-Olles, P. Slavik, N.K. Whitelaw, D.K. Smith, Self-assembled gels formed in deep eutectic solvents: supramolecular eutectogels with high ionic conductivity, Angew. Chem. Int. Ed 58 (2019) 4173–4178, https://doi.org/10.1002/anie.201810600.

[18] C. Padwal, H.D. Pham, S. Jadhav, T.T. Do, J. Nerkar, L.T.M. Hoang, A. Kumar Nanjundan, S.G. Mundree, D.P. Dubal, Deep eutectic solvents: green approach for cathode recycling of Li-ion batteries, Adv. Energy Sustain. Res 3 (2022), https://doi.org/10.1002/aesr.202100133.

[19] D. Julião, M. Xavier, X. Mascarenhas, Deep eutectic solvents: viable sustainable electrolytes for supercapacitors, Mater. Today Energy 42 (2024) 101432, https://doi.org/10.1016/j.mtener.2023.101432.

[20] G. Zante, M. Boltoeva, Review on hydrometallurgical recovery of metals with deep eutectic solvents, Sustain. Chem 1 (2020) 238–255, https://doi.org/10.3390/suschem1030016.

[21] C.M. Chabib, J.K. Ali, M.A. Jaoude, E. Alhseinat, I.A. Adeyemi, I.M. Al Nashef, Application of deep eutectic solvents in water treatment processes: a review, J. Water Process Eng 47 (2022) 102663, https://doi.org/10.1016/j.jwpe.2022.102663.

[22] M. Aslam, A. Rani, R. Singh, B. Nand, C. Verma, A. AlFantazi, G. Pandey, P. Singh, Harnessing deep eutectic solvents for advanced corrosion protection: a review, J. Mol. Liq 422 (2025) 126919, https://doi.org/10.1016/j.molliq.2025.126919.

[23] A. Gil-Villegas, A. Galindo, P.J. Whitehead, S.J. Mills, G. Jackson, A.N. Burgess, Statistical associating fluid theory for chain molecules with attractive potentials of variable range, J. Chem. Phys 106 (1997) 4168–4186, https://doi.org/10.1063/1.473101.

[24] T. Lafitte, A. Apostolakou, C. Avendaño, A. Galindo, C.S. Adjiman, E.A. Müller, G. Jackson, Accurate statistical associating fluid theory for chain molecules formed from Mie segments, J. Chem. Phys 139 (2013) 154504, https://doi.org/10.1063/1.4819786.

[25] S. Dufal, T. Lafitte, A.J. Haslam, A. Galindo, G.N.I. Clark, C. Vega, G. Jackson, The A in SAFT: developing the contribution of association to the Helmholtz free energy within a Wertheim TPT1 treatment of generic Mie fluids, Mol. Phys 113 (2015) 948–984, https://doi.org/10.1080/00268976.2015.1029027.

[26] J. Gross, G. Sadowski, Perturbed-chain SAFT: an equation of state based on a perturbation theory for chain molecules, Ind. Eng. Chem. Res 40 (2001) 1244–1260, https://doi.org/10.1021/ie0003887.

[27] J. Gross, G. Sadowski, Application of the perturbed-chain SAFT equation of state to associating systems, Ind. Eng. Chem. Res 41 (2002) 5510–5515, https://doi.org/10.1021/ie010954d.

[28] G.H. Hudson, J.C. McCoubrey, Intermolecular forces between unlike molecules a more complete form of the combining rules, Trans. Faraday Soc 56 (1960) 761–766, https://doi.org/10.1039/tf9605600761.

[29] J.S. Rowlinson, F.L. Swinton, The statistical thermodynamics of mixtures. Liq. Liq. Mix., Elsevier, 1982, pp. 279–315, https://doi.org/10.1016/b978-0-408-24193-9.50012-6.

[30] F.P. Pelaquim, R.G. Bitencourt, A.M.B. Neto, I.A.L. Dalmolin, M.C. da Costa, Carbon dioxide solubility in deep eutectic solvents: modelling using Cubic Plus Association and Peng-Robinson equations of state, Process Saf. Env. Prot 163 (2022) 14–26, https://doi.org/10.1016/j.psep.2022.04.075.

[31] A. Aminian, Modeling vapor–liquid equilibrium and liquid–liquid extraction of deep eutectic solvents and ionic liquids using perturbed-chain statistical associating fluid theory equation of state. Part II, AIChE J 68 (2022), https://doi.org/10.1002/aic.17774.

[32] C.H.J.T. Dietz, D.J.G.P. van Osch, M.C. Kroon, G. Sadowski, M. van Sint Annaland, F. Gallucci, L.F. Zubeir, C. Held, PC-SAFT modeling of CO2 solubilities in hydrophobic deep eutectic solvents, Fluid Ph. Equilib 448 (2017) 94–98, https://doi.org/10.1016/j.fluid.2017.03.028.

[33] E. Ali, M.K. Hadj-Kali, S. Mulyono, I. Alnashef, A. Fakeeha, F. Mjalli, A. Hayyan, Solubility of CO2 in deep eutectic solvents: experiments and modelling using the Peng-Robinson equation of state, Chem. Eng. Res. Des 92 (2014) 1898–1906, https://doi.org/10.1016/j.cherd.2014.02.004.

[34] R. Haghbakhsh, S. Raeissi, Modeling the phase behavior of carbon dioxide solubility in deep eutectic solvents with the Cubic Plus Association equation of State, J. Chem. Eng. Data 63 (2018) 897–906, https://doi.org/10.1021/acs.jced.7b00472.

[35] L.F. Zubeir, C. Held, G. Sadowski, M.C. Kroon, PC-SAFT modeling of CO2 solubilities in deep eutectic solvents, J. Phys. Chem. B 120 (2016) 2300–2310, https://doi.org/10.1021/acs.jpcb.5b07888.

[36] H. Ghanbari-Kalajahi, A. Haghtalab, High-pressure carbon dioxide solubility in a deep eutectic solvent (Choline Chloride/MDEA) + sulfolane—Experimental study and thermodynamic modeling using PC-SAFT equation of state, Fluid Ph. Equilib 580 (2024) 114040, https://doi.org/10.1016/j.fluid.2024.114040.

[37] I.I.I. Alkhatib, M.L. Ferreira, C.G. alba, D. Bahamon, F. Llovell, A.B. Pereiro, J.M. M. Araújo, M.R.M. Abu-Zahra, L.F. Vega, Screening of ionic liquids and deep eutectic solvents for physical CO2Absorption by soft-SAFT using key performance indicators, J. Chem. Eng. Data 65 (2020) 5844–5861, https://doi.org/10.1021/acs.jced.0c00750.

[38] K. Parvaneh, R. Haghbakhsh, A.R.C. Duarte, S. Raeissi, Investigation of carbon dioxide solubility in various families of deep eutectic solvents by the PC-SAFT EoS, Front. Chem 10 (2022), https://doi.org/10.3389/fchem.2022.909485.

[39] E. Cea-Klapp, I. Polishuk, R.I. Canales, H. Quinteros-Lama, J.M. Garrido, Estimation of thermodynamic properties and phase equilibria in systems of deep eutectic solvents by PC-SAFT EoS, Ind. Eng. Chem. Res 59 (2020) 22292–22300, https://doi.org/10.1021/acs.iecr.0c05109.

[40] F. Rabhi, F. Mutelet, H. Sifaoui, Solubility of carbon dioxide in carboxylic acid-based deep eutectic solvents, J. Chem. Eng. Data 66 (2021) 702–711, https://doi.org/10.1021/acs.jced.0c00844.

[41] R.M. Ojeda, F. Llovell, Soft-SAFT transferable molecular models for the description of gas solubility in eutectic ammonium salt-based solvents, J. Chem. Eng. Data 63 (2018) 2599–2612, https://doi.org/10.1021/acs.jced.7b01103.

[42] E.A. Crespo, L.P. Silva, J.O. Lloret, P.J. Carvalho, L.F. Vega, F. Llovell, J.A. P. Coutinho, A methodology to parameterize SAFT-type equations of state for solid precursors of deep eutectic solvents: the example of cholinium chloride, Phys. Chem. Chem. Phys 21 (2019) 15046–15061, https://doi.org/10.1039/c9cp02548k.

[43] J.O. Lloret, L.F. Vega, F. Llovell, Accurate description of thermophysical properties of tetraalkylammonium chloride deep eutectic solvents with the soft-SAFT equation of state, Fluid Ph. Equilib 448 (2017) 81–93, https://doi.org/10.1016/j.fluid.2017.04.013.

[44] O.H. Animasahun, M.N. Khan, C.J. Peters, Prediction of the CO2 solubility in deep eutectic solvents: a comparative study between PC-SAFT and cubic equations of state, in: Soc. Pet. Eng. - SPE Abu Dhabi Int. Pet. Exhib. Conf. 2017, SPE, 2017, https://doi.org/10.2118/188592-ms.

[45] S.H. Huang, M. Radosz, Equation of State for small, large, polydisperse, and associating molecules: extension to fluid mixtures, Ind. Eng. Chem. Res 30 (1991) 1994–2005, https://doi.org/10.1021/ie00056a050.

[46] P.J. Walker, H.W. Yew, A. Riedemann, Clapeyron.Jl: an extensible, open-source fluid thermodynamics toolkit, Ind. Eng. Chem. Res 61 (2022) 7130–7153, https://doi.org/10.1021/acs.iecr.2c00326.

[47] J.A. Barker, D. Henderson, Perturbation theory and equation of state for fluids. II. A successful theory of liquids, J. Chem. Phys 47 (1967) 4714–4721, https://doi.org/10.1063/1.1701689.

[48] J.A. Barker, D. Henderson, Perturbation theory and equation of state for fluids: the square-well potential, J. Chem. Phys 47 (1967) 2856–2861, https://doi.org/10.1063/1.1712308.

[49] T. Lafitte, M.M. Piñeiro, J.L. Daridon, D. Bessières, A comprehensive description of chemical association effects on second derivative properties of alcohols through a SAFT-VR approach, J. Phys. Chem. B 111 (2007) 3447–3461, https://doi.org/10.1021/jp0682208.

[50] N.M.P. Kakalis, A.I. Kakhu, C.C. Pantelides, Efficient solution of the association term equations in the statistical associating fluid theory equation of state, Ind. Eng. Chem. Res 45 (2006) 6056–6062, https://doi.org/10.1021/ie051417m.

[51] W.G. Chapman, G. Jackson, K.E. Gubbins, Phase equilibria of associating fluids chain molecules with multiple bonding sites, Mol. Phys 65 (1988) 1057–1079, https://doi.org/10.1080/00268978800101601.

[52] W.G. McMillan, J.E. Mayer, The statistical thermodynamics of multicomponent systems, J. Chem. Phys 13 (1945) 276–305, https://doi.org/10.1063/1.1724036.
[53] E.A. Müller, K.E. Gubbins, An equation of State for water from a simplified intermolecular potential, Ind. Eng. Chem. Res 34 (1995) 3662–3673, https://doi.org/10.1021/ie00037a055.
[54] P.J. Walker, X. Liang, G.M. Kontogeorgis, Importance of the relative static permittivity in electrolyte SAFT-VR mie equations of State, Fluid Ph. Equilib 551 (2022) 113256, https://doi.org/10.1016/j.fluid.2021.113256.
[55] S.H. Huang, M. Radosz, Equation of State for small, large, polydisperse, and associating molecules, Ind. Eng. Chem. Res 29 (1990) 2284–2294, https://doi.org/10.1021/ie00107a014.
[56] N.F. Carnahan, K.E. Starling, Equation of state for nonattracting rigid spheres, J. Chem. Phys 51 (1969) 635–636, https://doi.org/10.1063/1.1672048.
[57] H.A. Lorentz, Ueber die anwendung des Satzes vom Virial in der kinetischen Theorie der Gase, Ann. Phys 248 (1881) 127–136, https://doi.org/10.1002/andp.18812480110.
[58] D. Berthelot, Sur le mélange des gaz, Compt. Rendus 126 (1898) 15.
[59] N. Novak, G.M. Kontogeorgis, M. Castier, I.G. Economou, Modeling of gas solubility in Aqueous electrolyte solutions with the eSAFT-VR Mie equation of State, Ind. Eng. Chem. Res 60 (2021) 15327–15342, https://doi.org/10.1021/acs.iecr.1c02923.
[60] S. Anwer, I.I.I. Alkhatib, H.A. Salih, L.F. Vega, I. AlNashef, Investigating the role of water on CO2 capture by amine-based deep eutectic solvents through a combined experimental-molecular modeling approach, Sep. Purif. Technol 330 (2024) 125350, https://doi.org/10.1016/j.seppur.2023.125350.
[61] E.A. Crespo, J.M.L. Costa, A.M. Palma, B. Soares, M.C. Martín, J.J. Segovia, P. J. Carvalho, J.A.P. Coutinho, Thermodynamic characterization of deep eutectic solvents at high pressures, Fluid Ph. Equilib 500 (2019) 112249, https://doi.org/10.1016/j.fluid.2019.112249.
[62] K. Xin, M. Hashish, I. Roghair, M. van Sint Annaland, Process simulation and economic analysis of pre-combustion CO2 capture with deep eutectic solvents, Front. Energy Res 8 (2020), https://doi.org/10.3389/fenrg.2020.573267.
[63] H.D.B. Jenkins, H.K. Roobottom, J. Passmore, L. Glasser, Relationships among ionic lattice energies, molecular (formula unit) volumes, and thermochemical radii, Inorg. Chem 38 (1999) 3609–3620, https://doi.org/10.1021/ic9812961.
[64] G.M. Kontogeorgis, Chapter 6: association models-the CPA equation of state, Comput. Aided Chem. Eng (2004) 113–142, https://doi.org/10.1016/S1570-7946(04)80008-7.
[65] E.C. Voutsas, I.V. Yakoumis, D.P. Tassios, Prediction of phase equilibria in water/alcohol/alkane systems, Fluid Ph. Equilib 158–160 (1999) 151–163, https://doi.org/10.1016/s0378-3812(99)00131-4.
[66] H. Ghaedi, M. Ayoub, S. Sufian, A.M. Shariff, S.M. Hailegiorgis, S.N. Khan, CO2 capture with the help of phosphonium-based deep eutectic solvents, J. Mol. Liq 243 (2017) 564–571, https://doi.org/10.1016/j.molliq.2017.08.046.
[67] S. Kim, J. Chen, T. Cheng, A. Gindulyte, J. He, S. He, Q. Li, B.A. Shoemaker, P. A. Thiessen, B. Yu, L. Zaslavsky, J. Zhang, E.E. Bolton, PubChem 2023 update, Nucleic Acids Res 51 (2023) D1373–D1380, https://doi.org/10.1093/nar/gkac956.
[68] R.B. Leron, M.H. Li, High-pressure volumetric properties of choline chloride-ethylene glycol based deep eutectic solvent and its mixtures with water, Thermochim. Acta 546 (2012) 54–60, https://doi.org/10.1016/j.tca.2012.07.024.
[69] J. Wang, H. Cheng, Z. Song, L. Chen, L. Deng, Z. Qi, Carbon dioxide solubility in phosphonium-based deep eutectic solvents: an experimental and molecular dynamics study, Ind. Eng. Chem. Res 58 (2019) 17514–17523, https://doi.org/10.1021/acs.iecr.9b03740.
[70] L.F. Zubeir, D.J.G.P. Van Osch, M.A.A. Rocha, F. Banat, M.C. Kroon, Carbon dioxide solubilities in decanoic acid-based hydrophobic deep eutectic solvents, J. Chem. Eng. Data 63 (2018) 913–919, https://doi.org/10.1021/acs.jced.7b00534.
[71] R.B. Leron, M.H. Li, Solubility of carbon dioxide in a choline chloride-ethylene glycol based deep eutectic solvent, Thermochim. Acta 551 (2013) 14–19, https://doi.org/10.1016/j.tca.2012.09.041.
[72] A. Chiko, I. Polishuk, E. Cea-Klapp, J.M. Garrido, Comparison of cp-pc-saft and saft-vr-mie in predicting phase equilibria of binary systems comprising gases and 1-alkyl-3-methylimidazolium ionic liquids, Molecules 26 (2021) 6621, https://doi.org/10.3390/molecules26216621.
[73] J.S. Andreu, L.F. Vega, Capturing the solubility behavior of CO2 in ionic liquids by a simple model, J. Phys. Chem. C 111 (2007) 16028–16034, https://doi.org/10.1021/jp074353x.
[74] C.S. Beraldo, X. Liang, L.A. Follegatti-Romero, Predicting the solubility of gases in imidazolium-based ionic liquids with SAFT-VR Mie EoS by a novel approach based on COSMO, Chem. Eng. Sci 285 (2024) 119610, https://doi.org/10.1016/j.ces.2023.119610.
[75] S.H. Khudaida, M. Kfoury, J. Liu, A.H. Tiwikrama, S. Fourmentin, A step forward in supramolecular green solvents characterization: total vapor pressure determination, J. Mol. Liq 427 (2025) 127377, https://doi.org/10.1016/j.molliq.2025.127377.
[76] J. Wu, N. Wei, X. Chen, R. Zhang, X. Chen, J. Tong, Determination of vapor pressure, evaporation enthalpy and polarity of imidazolium-based ionic liquids, J. Therm. Anal. Calorim 149 (2024) 5511–5522, https://doi.org/10.1007/s10973-024-13107-6.
[77] J.-A. Mejía-de-Dios, E. Mezura-Montes, A new evolutionary optimization method based on center of Mass, Decis. Sci. Action (2019) 65–74, https://doi.org/10.1007/978-981-13-0860-4_6.
[78] J.-A. Mejía-de-Dios, E. Mezura-Montes, Metaheuristics: a Julia package for single- and multi-objective optimization, J. Open Source Softw 7 (2022) 4723, https://doi.org/10.21105/joss.04723.
[79] J. Bezanson, A. Edelman, S. Karpinski, V.B. Shah, Julia: a fresh approach to numerical computing, SIAM Rev 59 (2017) 65–98, https://doi.org/10.1137/141000671.
[80] A.P. Carneiro, C. Held, O. Rodríguez, G. Sadowski, E.A. Macedo, Solubility of sugars and sugar alcohols in ionic liquids: measurement and PC-SAFT modeling, J. Phys. Chem. B 117 (2013) 9980–9995, https://doi.org/10.1021/jp404864c.
[81] X. Ji, C. Held, G. Sadowski, Modeling imidazolium-based ionic liquids with ePC-SAFT, Fluid Ph. Equilib 335 (2012) 64–73, https://doi.org/10.1016/j.fluid.2012.05.029.
[82] C. Tsioptsias, I. Tsivintzelis, C. Panayiotou, Equation-of-state modeling of mixtures with ionic liquids, Phys. Chem. Chem. Phys 12 (2010) 4843–4851, https://doi.org/10.1039/c000208a.
[83] D. Bedrov, J.P. Piquemal, O. Borodin, A.D. MacKerell, B. Roux, C. Schröder, Molecular dynamics simulations of ionic liquids and electrolytes using polarizable force fields, Chem. Rev 119 (2019) 7940–7995, https://doi.org/10.1021/acs.chemrev.8b00763.
[84] P.A. Hunt, C.R. Ashworth, R.P. Matthews, Hydrogen bonding in ionic liquids, Chem. Soc. Rev 44 (2015) 1257–1288, https://doi.org/10.1039/c4cs00278d.
[85] S. Rozas, A. Gutiérrez, M. Atilhan, A. Bol, S. Aparicio, Understanding the CO2 capture potential of tetrapropylammonium-based multifunctional deep eutectic solvent via molecular simulation, J. Mol. Liq 393 (2024) 123416, https://doi.org/10.1016/j.molliq.2023.123416.
[86] U.L. Abbas, Y. Zhang, J. Tapia, S. Md, J. Chen, J. Shi, Q. Shao, Machine-learning-assisted design of deep eutectic solvents based on uncovered hydrogen bond patterns, Engineering 39 (2024) 74–83, https://doi.org/10.1016/j.eng.2023.10.020.
[87] P. Kalhor, J. Xu, H. Ashraf, B. Cao, Z.W. Yu, Structural properties and hydrogen-bonding interactions in binary mixtures containing a deep-eutectic solvent and acetonitrile, J. Phys. Chem. B 124 (2020) 1229–1239, https://doi.org/10.1021/acs.jpcb.9b10751.
[88] C. Ma, A. Laaksonen, C. Liu, X. Lu, X. Ji, The peculiar effect of water on ionic liquids and deep eutectic solvents, Chem. Soc. Rev 47 (2018) 8685–8720, https://doi.org/10.1039/c8cs00325d.
[89] D. Peng, Z. Yu, A. Alhadid, M. Minceva, Modeling the viscosity of ChCl-based deep eutectic solvents and their mixtures with water, Ind. Eng. Chem. Res 63 (2024) 1623–1633, https://doi.org/10.1021/acs.iecr.3c03652.
[90] W.G. Chapman, K.E. Gubbins, G. Jackson, M. Radosz, SAFT: equation-of-state solution model for associating fluids, Fluid Ph. Equilib 52 (1989) 31–38, https://doi.org/10.1016/0378-3812(89)80308-5.
[91] R. Haghbakhsh, S. Raeissi, A.R.C. Duarte, Group contribution and atomic contribution models for the prediction of various physical properties of deep eutectic solvents, Sci. Rep 11 (2021) 6684, https://doi.org/10.1038/s41598-021-85824-z.
[92] Y. Xu, R. Shahriari, Prediction of second order derivative thermodynamic properties of ionic liquids using SAFT-VR Morse equation of state, Fluid Ph. Equilib 549 (2021) 113204, https://doi.org/10.1016/j.fluid.2021.113204.
[93] C.S. Beraldo, X. Liang, L.A. Follegatti-Romero, Predicting imidazolium ionic liquid properties with a simple molecular volume-based SAFT-VR Mie approach, Chem. Eng. Sci 301 (2025) 120748, https://doi.org/10.1016/j.ces.2024.120748.